

# The urban heat island and thermal heat stress correlate with climate dynamics and energy budget variations in multiple urban environments



Nurul Syahira Mohammad Harmay<sup>a,b</sup>, Minha Choi<sup>c,d,\*</sup>

<sup>a</sup> School of Civil, Architectural and Environmental System Engineering, Sungkyunkwan University, Suwon, 440-746, Republic of Korea

<sup>b</sup> Department of Global Smart City, Sungkyunkwan University, Suwon, 440-746, Republic of Korea

<sup>c</sup> School of Civil, Architectural Engineering and Landscape Architecture, Sungkyunkwan University, Suwon, 440-746, Republic of Korea

<sup>d</sup> Department of Water Resources, Graduate School of Water Resources, Sungkyunkwan University, Suwon, 440-746, Republic of Korea

## ARTICLE INFO

### Keywords:

Urban heat island  
Urban overheating  
Thermal heat stress  
Energy balance  
United States

## ABSTRACT

Rising temperatures that occur in cities resulted in the urban heat island (UHI) which could also amplify the thermal heat stress, leading to climate-related human mortality. Our study investigated the UHI effect and thermal heat stress of heat index (HI) in the U.S. cities of arid, continental, temperate, and tropical climate zones. A long-term simulation of the UHI and HI was conducted using Community Land Model version 5.0 from 1990 to 2014. The relationship between UHI and HI with climate and energy flux variables are analyzed with divided study periods (1990–2000 and 2001–2014) for the urban impact assessment. Higher sensible heat was reported, particularly in the arid and tropical cities. Further, temperate climate showed increasing annual trends for UHI and  $\Delta$ HI (urban-rural difference of HIs). The later period (2001–2014) demonstrated greater UHI and  $\Delta$ HI trends, implying a notable change in climate and urban expansion. The UHI, ranging from 0.73 °C to 2.07 °C, was more intense compared with  $\Delta$ HI, at 0.14 °C to 1.23 °C. The UHI was positively correlated with temperatures in hot cities, while precipitation is the main driver in the continental city. For  $\Delta$ HI, the relationship with temperatures were dominant in all climate zones.

## 1. Introduction

Climate change has increased the Earth's surface temperature due to rising levels of atmospheric carbon dioxide, which can affect other climatic variables. Considering recent climate trends, urban residents are expected to be the most likely to be exposed to the enhanced thermal risks which may also affect human health (McMichael et al., 2006). Despite covering a small percentage of the global surface, cities consume nearly 70% of the energy produced worldwide (International Energy Agency, 2008). Previous studies have examined mitigation frameworks with respect to mitigate climate change and creating more resilient urban environments that can adapt to climate-driven extreme events (Boyd et al., 2022; Nematchoua et al., 2018; Salimi & Al-Ghamdi, 2020). Energy consumption in cities produces water vapor, pollution, and waste heat, each of which directly affects air quality, humidity, temperature, and human health (Quah & Roth, 2012). Recently, Nguyen et al. (2022) reported notable climate change influences based on extreme temperature variations in Southeast Asian cities over the past three decades, that are exacerbating the heat island effects. Further,

Qiao et al. (2022) argued that future climate change will have large impact on cities' maintenance costs and the end-of-life phases in the U.S. Table 1.

The escalation of human activities and the expansion of dense built environments have resulted in remarkable differences of temperatures between urban and surrounding rural areas, which is known as the urban heat island (UHI) effect (Oke, 1973). The alteration of land cover has led to warmer conditions in urban areas due to the replacement of vegetated ground with buildings and pavement which have also intensified the UHI effects (Adams & Smith, 2014; Mirzaei & Haghhighat, 2010; Phelan et al., 2015). Recent studies have concluded that the UHI intensity has increased significantly between 1990 and 2010 due to urban growth and limited green infrastructure in the city core, and predicted that this trend will continue through at least 2030 (Shen et al., 2022; Tian et al., 2021). Besides, higher impervious surfaces in urban areas may modify surface-energy budgets, which include heat storage flux, evaporative reduction, anthropogenic heat release, and sensible heat fluxes (Oke, 1982; Zhao et al., 2014). The conversion of natural landscapes into built-up areas is also related to higher sensible heat

\* Corresponding author at: School of Civil, Architectural Engineering and Landscape Architecture, Sungkyunkwan University, Suwon 440-746, Republic of Korea.  
E-mail addresses: [nurulharmay@g.skku.edu](mailto:nurulharmay@g.skku.edu) (N.S. Mohammad Harmay), [mhchoi@skku.edu](mailto:mhchoi@skku.edu) (M. Choi).

fluxes which resulted in higher emission of longwave radiation, hence will enhance the UHI effect (Coutts et al., 2007).

According to the U.S. Environmental Protection Agency, the “heat island effect” can increase urban temperatures by 1.00 °C to 3.00 °C in cities with more than 1 million residents compared to surrounding rural areas, and the difference can be as much as 12.00 °C, depending on the geographical location (Arnfield, 2003). Kenward et al. (2014) have shown that the magnitude of the UHI in U.S. cities varies according to regional and local characteristics. With regard to climate conditions, the low relative humidity, clear skies, and low wind speeds can enhance the UHI (Gedzelman et al., 2003; Santamouris, 2016). An analysis of extreme heat events has indicated that the UHI effect can amplify mortality and morbidity rates through high urban temperatures, radiation effects, humidity, urban pollution, and the variability of wind (Conti et al., 2005). A discrete characteristic of the urban diurnal temperature may increase the risks to human health due to heat stress because it withholds the cooling effects in the cities (McElroy et al., 2020). Additionally, these conditions also reduce labor productivity and weakened individual well-being, leading to significant economic losses (Zander et al., 2018). In the U.S., heat-related conditions are the largest cause of mortality among natural disasters, compared with flooding, hurricanes, and typhoons. Hence, the amplification of urban temperatures, combined with the urban effects on humidity, radiation, and other climatic conditions should therefore be mitigated to reduce the threats to human health (Fischer et al., 2012).

Numerous efforts have been made to quantify both the UHI effect and heat-stress characteristics using ground observations, satellite data, and model simulations (Chakraborty et al., 2020; Jin, 2012). Studies of extreme heat events based on the heat index (HI) mechanism using the in-situ weather stations can only provide a short-term analysis (Suparta & Yatim, 2017; Wang et al., 2021a). Recently, Kumar et al. (2022) analyzed heat waves and heat-stress patterns with a gridded meteorological dataset. Their study has evaluated the degree of discomfort and categorized the heat stress level, without considering the relationship with the land surface variables associated with the energy fluxes cycle. With the advancement of land surface models (LSMs), hydrometeorological flux and energy cycles can be simulated, along with the UHI effect and heat-stress characteristics. The Community Land Model (CLM) is an LSM component that examines the chemical, physical, and biological processes involved in climate interactions (Oleson & Bonan, 2010). Using surface data enhancement of urban parameterization in the CLM, several improvements have been made to simulate the local climates of urban areas with an evidence from the recent studies of UHI using CLM version 4.0 (Zhao et al., 2014; Mohammad Harmay et al., 2021b), heat stress metrics from CLM version 4.5 (Buzan et al., 2015), and the validation of urban flux tower dataset based on CLM version 5.0 (Oleson & Feddema, 2020).

Previous studies have investigated the urban characteristics related to UHI, heat stress, urban climate, and urban energy cycles. However, few studies have addressed these components together. Kim et al. (2018), who examined the effect of UHIs using an urban canopy model, reported that UHI intensity varied from 1.25 °C to 4.35 °C in multiple climate zones in the U.S. However, their study did not discuss the climate factors that influence the development of UHIs. Another study reported the positive trend of UHIs, along with their responses to weather conditions (Si et al., 2022). While this study revealed significant correlations between UHIs and solar duration, relative humidity, and

rainfall, the mechanism of UHI with urban energy cycles were not fully addressed due to some limitations from satellite dataset that could only provide few climatic variables and land cover information. On the other hand, the long-term simulations of energy-flux variables remain inadequate, and most such studies provide only short-term estimates of energy fluxes and climate variables in cities (Chew et al., 2021; Demuzere et al., 2013). Additionally, research on heat stress metrics based on numerical modeling that combines the effects of temperature, humidity, and urbanization are still scarce (Oleson et al., 2015; Sherwood & Huber, 2010). Wang et al. (2021b) elaborated the impact on various urban structure types on heat stress influenced; however, the urban heat stress studies based on Local Climate Zones classification provides a few shortcomings that lies on the combined urban structure. Climate and hydrometeorological variations are also frequently overlooked in studies of urban heat stress (Eldesoky et al., 2022). Therefore, there is an urgent need to better understand the mechanism of heat stress in relation with climate change and urbanization impact.

The major objective of this study was to examine the attributes of UHIs and heat stress in four heterogenous American cities (Phoenix, Minneapolis, Houston, and Miami), that represent arid, continental, temperate, and tropical climate zones, respectively. These selected cities were classified under the same building classification of “open low-rise” to avoid the combined urban structure effects on the quantification of heat stress. Our specific research questions and objectives were: a) How do energy fluxes and climate variables relate to different climate zones and urban characteristics between 1990 and 2014? b) What are the regional climate conditions’ effects on the development of the UHI effect and heat stress? To address these questions, the recently updated CLM version 5.0 (CLM5.0) with urban parameterizations was utilized to estimate water and energy fluxes in the four selected cities. Available urban flux tower observations were used to validate the simulated model outputs from 1990 to 2014. Statistical metrics were applied to analyze the long-term trends in air temperature ( $T_a$ ), surface temperature ( $T_s$ ), sensible heat flux (H), and latent heat flux (LE) over the four cities. Next, the seasonal variations of urban temperature and thermal heat stress denoted by  $T_{urban}$  and  $HI_{urban}$  were investigated, along with the climate variability. Further analysis was conducted to provide details about the urban-rural temperature differences indicated by UHI and urban-rural HI differences indicated by  $\Delta HI$ , and their relationship with climatic influences and energy fluxes. The analysis was performed during divided study periods (1990–2000 and 2001–2014) for the urban impact assessment.

## 2. Study area and dataset

### 2.1. Study area

As shown in Fig. 1, four cities in the conterminous United States were selected to represent different climate characteristics based on the Köppen-Geiger climate classifications: arid (Phoenix); continental (Minneapolis), temperate (Houston), and tropical (Miami). The cities were chosen based on the availability of urban flux tower dataset for model validation which are Phoenix and Minneapolis. The study areas were also selected in cities that have different climate zones, but having similar building characteristics which is “open low-rise” since we wanted to avoid variances caused by different local climate zones (LCZs) characteristics (Stewart & Oke, 2012). Additionally, these are the cities

**Table 1**  
Meteorological and field characteristics of selected cities.

City	State	Latitude	Longitude	Elevation	Climate type	Mean annual temperature	Mean annual precipitation
Phoenix	Arizona	33.48° N	112.14° W	331 m	‘BWh’ (arid)	24.00°C	204 mm
Minneapolis	Minnesota	45.00° N	93.19° W	253 m	‘Dfa’ (continental)	7.90°C	869 mm
Houston	Texas	29.76° N	95.36° W	32 m	‘Cfa’ (temperate)	18.50°C	1264 mm
Miami	Florida	25.77° N	80.20° W	2 m	‘Am’ (tropical)	25.03°C	1573 mm

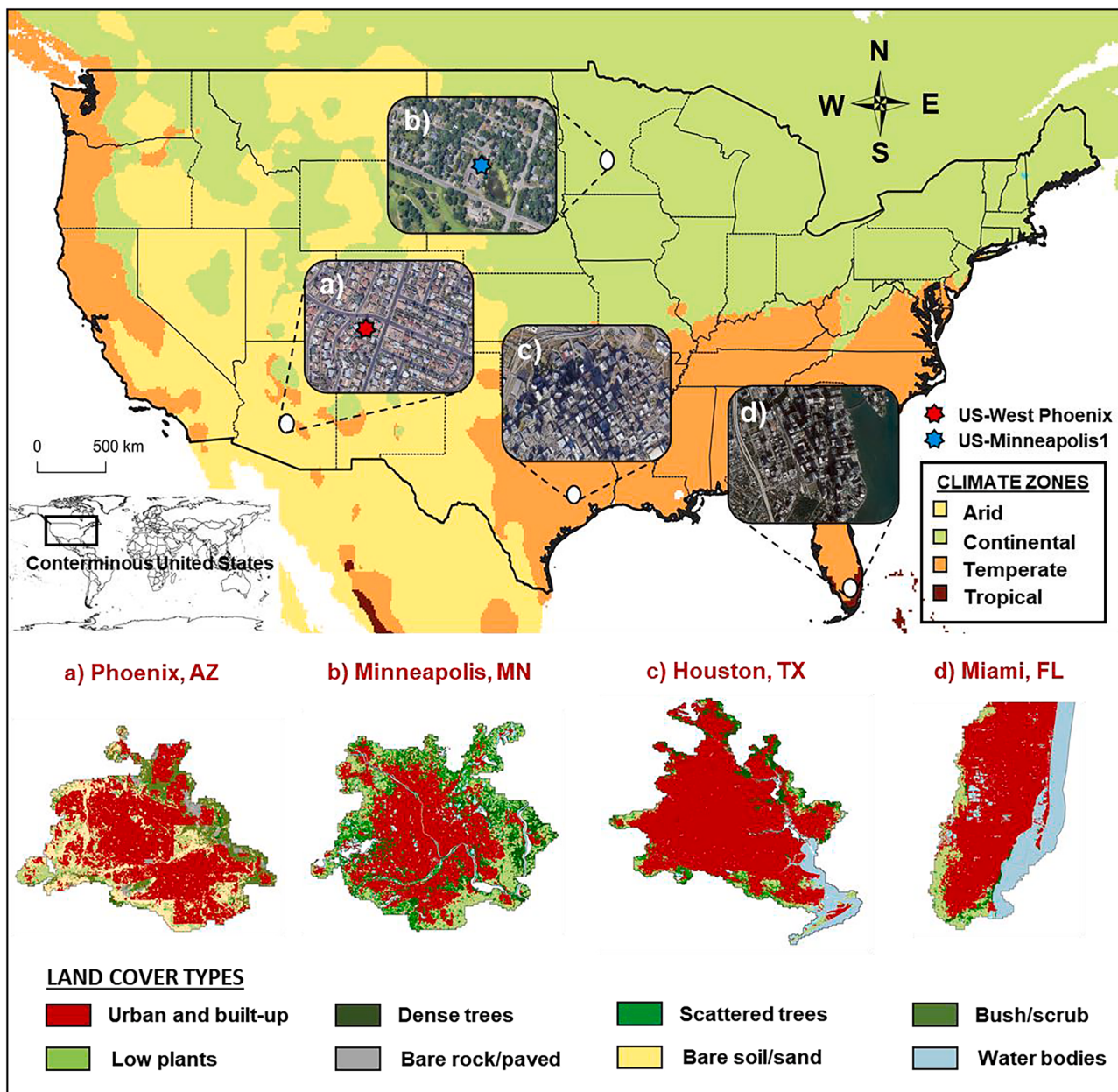


Fig. 1. Location of selected cities over the conterminous United States based on climate zones and land cover classifications.

that experienced the greatest heat-related mortality over the last 15 years in the U.S (Vaidyanathan et al., 2020).

Phoenix has a hot and arid climate, with extremely dry and hot summers, giving it a Köppen-Geiger classification of 'BWh'. The highest average annual temperature is 31.00 °C, with temperatures peaking in late June through July. A major metropolitan area in the state of Arizona, Phoenix has experienced rapid urbanization in the 20th century as developers converted agricultural land into urban and suburban developments (Jenerette et al., 2011). The average daily temperature in Phoenix has increased by 3.10 °C, reaching the "misery hours per day" range that negatively affects humans and socioeconomic conditions (Baker et al., 2002). Recently, a notable increase in heat was also found to potentially expose more than 1 million residents to hazardous level of heat (Stone et al., 2021).

Minneapolis has a humid continental climate that is classified as 'Dfa' according to the Köppen classification scheme. It experiences extreme weather phenomena, including tornadoes, strong winds, blizzards, and heavy snow. This city has an average temperature of

-11.55 °C in winter and 21.44 °C in the summer, with an average temperature of 7.40 °C and 747 mm of precipitation annually. This city has a density of approximately 1000 inhabitants and 350 housing density units per square kilometer (Radeloff et al., 2005). Due to the climate and its location near the metropolitan region, this city is prone to UHI effects (Roy & Yuan, 2009). Previous studies also demonstrated that the urban temperature in Minneapolis city is getting warmer due to a lack of green areas in specific zones (i.e. railroads, industrial) (Mbuh et al., 2021).

The metropolitan area of Houston, which has a climate classification of humid subtropical climate ('Cfa') is exposed to extreme heat due to warm and humid conditions, resulting in high temperatures and an intense UHI effect (Papalexiou et al., 2018; Zhao et al., 2014). Besides, Houston is considered as one of the fastest growing and rapidly diversifying metropolitan areas in the U.S. (Emerson et al., 2012). An increasing population and expansion of urban areas in Houston may affect urban thermal characteristics, which will consequently influence future urban hazards in this city (Conlon et al., 2016).

Miami, the most populous city in Florida, is located on the southeastern coast of the U.S. This city has a tropical climate ('Am') with an annual temperature of 25.03 °C and 1573 mm of annual precipitation. Miami covers more than 145.20 km<sup>2</sup>, with 93.00 km<sup>2</sup> consisting of land and 52.00 km<sup>2</sup> of water. Over the last 30 years, the coastal counties of the southeastern U.S have experienced unusual growth, with a recorded 64% population increase between 1970 and 1990. It is expected that the majority of future population growth will occur along the coast, which is associated with economic development and in-migration of retirees and job-seekers (Scott et al., 2006). Because Miami is on the coast, this city can only be expanded in northward or westward, making it more populated due to the urbanization and urban development (Divya et al., 2021).

Despite the individual cities that were selected in this study, our work provides a long-term analysis based on the climate model simulation from 1990 to 2014 which incorporated the effects of UHI and HI in each city based on the climate variations, energy fluxes response, and urban land cover changes. The understanding of the land-surface energy balance variation is important since it may affect the energy cycle of the climate system and therefore alter the climate conditions (Zhang et al., 2014). Additionally, the surface energy budget components are also being used to describe the climate change process in multiple climate zones (Andrews et al., 2009).

## 2.2. Dataset

### 2.2.1. Urban flux tower

To validate the model simulation, this study used the available urban flux tower located at Maryvale in the city of Phoenix. The eddy-covariance flux tower was installed at an elevation of approximately 22.86 m for flux measurements. The Webb–Pearmann–Leuning method was applied to enhance the density effect of water and heat fluxes on flux tower data (Webb et al., 1980). Data from this site were provided from January 2012 to December 2012 at a resolution of 30 min and upscaled to 1 h to adhere to the outputs from the CLM.

Another selected urban flux tower was located in a suburban neighborhood of Minneapolis–Saint Paul, in east-central Minnesota (Menzer & McFadden, 2017). Flux measurements were obtained from the 40.00 m tall KUOM broadcast tower at a residential neighborhood consisting primarily of detached housing and a recreational golf course. Carbon and water flux data from this site were provided from January 2007 to May 2009, and were upscaled from a half-hourly to an hourly dataset.

## 3. Methods

### 3.1. Model description

The CLM was developed at the National Center for Atmospheric Research (NCAR) to incorporate biogeophysical and biogeochemical parameterizations of the Earth's surface into a model of the land and atmosphere. The CLM provides long-term simulations of future climate projections and water and energy fluxes, particularly in regions with limited in situ data (Lawrence et al., 2012). This study used the most recent version of CLM5.0, with the addition of urban parameterization, which is called the Community Land Model Urban (CLMU) that has received numerous surface-data improvements since 2018 (Oleson & Feddema, 2020). The urban land unit in the model is represented as different columns, such as sunlit and shaded walls, pervious and impervious canyon surfaces, and roofs, based on the canyon concept developed by Oke and Cleugh (1987). The newly improved CLMU in CLM5.0 has an increased capability to identify urban density classes and urban radiative and turbulent flux (Oleson & Feddema, 2020). The model uses gridded 0.5° Global Soil Wetness Project Phase 3 for the forcings which includes the three-hourly meteorological parameters of air temperature, precipitation, solar radiation, wind speed, humidity,

and atmospheric pressure. The CLM model were analyzed from 1990 to 2014, with a total of five runs of 25-year simulations (125 years); the first four runs were used to spin up the model for the output parameters to reach the equilibrium stage, and the last run was used for the analysis. The simulation was conducted on a finite volume grid of 0.5° × 0.5° using an atmospheric boundary condition provided by NCAR. Monthly output variables were used for further seasonal and annual UHI and HI quantification.

### 3.1.1. Model performance

Statistical analysis tools, including the Pearson correlation coefficient (R), root mean square error (RMSE), mean bias error (MBE), index of agreement (IOA), and mean absolute error (MAE) were used to validate the climate and energy fluxes parameters from CLM5.0 with observations from flux towers.

$$R = \frac{\sum_{i=1}^n (C_i - \bar{C})(O_i - \bar{O})}{\sqrt{\sum_{i=1}^n (C_i - \bar{C})^2} \sqrt{\sum_{i=1}^n (O_i - \bar{O})^2}}, \quad (1)$$

$$RMSE = \sqrt{\frac{\sum_{i=1}^n (C_i - O_i)^2}{n}}, \quad (2)$$

$$MBE = \frac{\sum_{i=1}^n (C_i - O_i)}{n}, \quad (3)$$

$$IOA = 1 - \frac{\sum_{i=1}^n (C_i - O_i)^2}{\sum_{i=1}^n (|C_i - \bar{O}| + |O_i - \bar{O}|)^2}, \quad (4)$$

$$MAE = \frac{1}{n} \sum_{i=1}^n |C_i - O_i|, \quad (5)$$

where  $C_i$  and  $O_i$  represent CLM-based and observed values, respectively, while the mean of the CLM output and observed data are denoted by  $\bar{O}$  and  $\bar{C}$ , respectively.

### 3.2. Urban heat island effect

In general, the UHI effect can be explained as the temperature difference between urban and surrounding rural areas. In this study, quantification of UHI followed the definition by Zhao et al. (2014), who employed climate modeling to estimate UHI intensity by distinguishing urban and rural fractions in each grid cell. Because this study used the NCAR Community Earth System Model simulation, the design of the CLM5.0 model allowed for urban and rural components in each grid cell, with the rural components characterized by vegetated surfaces that were analyzed separately for intercomparisons. To construct the UHI element, urban and rural variables were obtained from the model output at each grid cell where the selected cities were located, and the UHI intensity defined as:

$$UHI = T_{urban} - T_{rural} \quad (6)$$

where  $T_{urban}$  is the temperature in the urban pixel and  $T_{rural}$  is the temperature in the rural pixel. The simulation was conducted at a global scale, with site-level data extracted by CLM5.0 scripts and tools. Both annual and seasonal mean UHI from 1990 to 2014 were quantified as the mean temperature differences between urban and rural boundary areas in each grid cell. Finally, we used the air temperature variable for UHI quantification to be consistent with parameter used in heat stress calculations (Section 3.3).

### 3.3. Heat stress modeling

There are several heat stress indices that include the temperature and additional environmental factors. In this study, we used the HI

developed by the U.S. National Weather Service (NWS), which was quantified using the model simulation to analyze the heat stress and urban characteristics involved in climate dynamics. Since this study was conducted in the cities of the U.S., the NWS HI is the most favorable option, and correlated with the heat-related mortality (Davis et al., 2003). The version of CLM5.0 used in this study also applies new urban classifications and parameters that include the heat-stress indices module from the NWS HI (Oleson & Feddema, 2020). The advantages of NWS HI have also been proved by previous studies. Dahl et al. (2019) used the NWS HI to define the risk threshold for public heat alerts in the U.S. Research conducted by Golden et al. (2008) in Phoenix found that the greatest incidence of heat-related events occurred during periods of elevated human comfort indices, represented by HI. The application of NWS HI is not limited to the U.S continent, and the index has also been utilized for heat-related studies in Asia (e.g., Malaysia, Vietnam), South Africa, and Europe (Fischer & Schär, 2010; Opitz-Stapleton et al., 2016; Orimoloye et al., 2017; Suparta & Yatim, 2017).

The HI from the NWS required an early warning system of heat stress, and the index was developed as a polynomial fit to Steadman's (Steadman, 1979) comfort model (Rothfusz, 1990) as follows:

$$\begin{aligned} HI = & -42.379 + 2.04901523T_a + 10.14333127RH - 0.22475541T_aRH \\ & - 6.83738 \times 10^{-3}T_a^2 - 5.481717 \times 10^{-2}RH^2 + 1.22874 \\ & \times 10^{-3}T_a^2RH + 8.5282 \times 10^{-4}T_aRH^2 - 1.99 \times 10^{-6}T_a^2RH^2 \end{aligned} \quad (7)$$

where RH is relative humidity and  $T_a$  is air temperature. The HI was calculated as degrees Celsius in this study to standardize it with other parameters for further analysis. Details of the HI assumptions considered in the model can be found in Rothfusz (1990). Based on the iterative procedure from the assumed magnitudes, the regression model was reduced to a relationship between temperature and the human resistance to heat and moisture transfer. The HI was categorized according to the NWS to determine the heat-stress level as follows: 27.00 °C to 32.00 °C represents caution; 33.00 °C to 39.00 °C extreme caution, 40.00 °C to 51.00 °C danger, and  $\geq 52.00$  °C extreme danger.

The module chosen for heat-stress indices was initially developed by Buzan et al. (2015) and was calculated online using the previous release of CLM (version 4.5). These indices were quantified from combinations of simulated air temperature, humidity, and, in some cases, wind speed. In CLM5.0, heat-stress metrics are calculated directly at the sub-grid scale in multiple environments. Additionally, considering the impact of heat stress in both urban and rural areas, HI was calculated as the corresponding difference between urban and rural areas in this study as follows:

$$\Delta HI = HI_{urban} - HI_{rural} \quad (8)$$

### 3.4. Mann-Kendall and Sen slope trend analysis

A non-parametric Mann-Kendall test was used for time series detection of the outputs from the model simulation (Kendall, 1938; Mann, 1945). For non-parametric statistical analysis, positive statistics indicate an increasing trend, while negative statistics indicate a negative trend. The null hypothesis assumed that the set of data were randomly ordered with no significant trend, while a significant trend was determined if the p-value was less than 0.05 (\*) and 0.01 (\*\*). The slope for each data series was also estimated based on each pair in the dataset, following Sen (1968).

## 4. Results and discussion

### 4.1. Validation of CLM5.0 with urban flux tower data

This study involved the long-term urban and energy budget analysis for 1990 to 2014. In conjunction to this, the climate model simulations

from CLM5.0 were performed due to its robustness to provide multiple set of hydrometeorological parameters in a larger temporal scale. In order to verify the model accuracy, the simulated outputs were first validated with the observed data from Minneapolis and Phoenix. Fig. 3 and Table 2 showed the monthly time series and statistical comparisons of R, IOA, MBE, RMSE, and MAE for  $T_a$ , H, and LE at two different urban sites of US-Minneapolis1 and US-West Phoenix with CLM5.0 and flux tower data.

For the estimation of  $T_a$ , both sites demonstrated a high degree of agreement, with R values of 0.97 and 0.99 for US-Minneapolis1 and US-West Phoenix, respectively (Table 2). This may due to the high temporal and spatial resolution of the precipitation parameter in the CLM, which was the main factor that increased the model accuracy for the comparison with observed data (Kokkonen et al., 2018). Meanwhile, arid city demonstrated a relatively high negative bias of  $-7.87$  °C for MBE and high MAE of 7.37 °C which could be due to the limited urban parameterization of the model. For instance, the anthropogenic heat flux that only incorporates conventional variables in the climate model can underestimate the simulated temperature variables in the warmer urban boundary layer (Fig. 3b, Table 2) (Cao et al., 2016). Besides, more space heating is required at high latitudes but the model only considered limited heat synergistic effects, which potentially causing an underestimate of temperature in hot climates (Oleson & Feddema, 2020).

The surface-energy budget parameters of H and LE from CLM5.0 were also validated with the observed dataset for further urban analysis (Fig. 3c-f). Based on the time-series results, values for H were higher at both sites compared with those for LE, which is consistent with a previous urban study based on a CLM (version 4) simulation (Mohammad Harmay & Choi, 2021a). The sensible heat was higher than the latent heat due to the landscape features of both sites, which are located in urbanized areas, because large urbanized areas that have a higher percentage of natural land that has been converted to developed land may result in changes in thermal, aerodynamic, moisture, and radiation parameters (Silva et al., 2018). As shown in Table 2, the continental city (US-Minneapolis1) exhibited the most promising results for the estimation of H, with R and IOA values of 0.92 and 0.93, respectively. The MAE also showed lower value of  $8.61 \text{ W m}^{-2}$  at US-Minneapolis1 compared to the US-West-Phoenix. Meanwhile, both sites showed a negative MBE for H, at  $-3.19 \text{ W m}^{-2}$  and  $-17.54 \text{ W m}^{-2}$  for US-Minneapolis1 and US-West Phoenix (Table 2), respectively, possibly due to the forcing data and the model uncertainty (Oleson & Feddema, 2020).

For LE estimates of the arid city (US-West Phoenix), CLM5.0 produced a higher degree of agreement, with R and IOA values of 0.83 and 0.88, respectively, compared with the continental city (Table 2). The simulated LE also demonstrated a small MBE of  $0.47 \text{ W m}^{-2}$  at the US-West Phoenix site compared with US-Minneapolis1 (Table 2). Meanwhile, the model underestimated the LE in the continental city (US-Minneapolis1), with a negative bias of  $-28.00 \text{ W m}^{-2}$  (Table 2). At this site, the underestimation was observed during episodes of heavy rainfall (Fig. 3e). Because US-Minneapolis1 experienced greater rainfall intensity due to its continental climate, higher amounts of the available water on the surface increased the energy used for evaporation and converted it to latent heat, as shown by the higher LE from the flux tower

**Table 2**

Statistical results for air temperature ( $T_a$ ), sensible heat flux (H), and latent heat flux (LE) between observations and simulated variables from CLM. Units: [ $T_a$  (°C); H, LE ( $\text{W m}^{-2}$ )] for MBE, RMSE and MAE.

Variables	Validation site	R	IOA	MBE	RMSE	MAE
$T_a$	US-Minneapolis1	0.97	0.93	5.10	6.93	5.62
	US-West Phoenix	0.99	0.83	-7.87	8.08	7.37
H	US-Minneapolis1	0.92	0.93	-3.19	11.36	8.61
	US-West Phoenix	0.82	0.81	-17.54	23.93	19.51
LE	US-Minneapolis1	0.77	0.56	-28.00	32.89	31.02
	US-West Phoenix	0.83	0.88	0.47	5.40	3.87

observations. Additionally, previous findings reported that the tile approach in a single-layer urban canopy model can lead to an underestimation of latent heat flux especially during the high cloud coverage (Demuzere et al., 2013). The LE parameterization in the CLM model that mostly depended on the roof and impervious surface evaporation was usually generated rapid evaporation in the model during the high sun-light conditions, compared to the non-clear sky conditions. Overall, the long-term simulated parameters from CLM5.0 demonstrated favorable results with the in-situ observations, making the model suitable for the further analysis.

#### 4.2. Temporal trends in climate characteristics and surface-energy budgets

The climate characteristics and surface-energy budgets in each climate zone were represented by  $T_a$ ,  $T_s$ , H, and LE. Air temperature and surface temperature variables are among the most useful parameters for describing urban heat and thermal characteristics (i.e., the UHI effect, heat stress, and heat waves) (Edmondson et al., 2016; Watkins et al., 2007). Additionally, H and LE, that represent the surface-energy budget distributions, are also known as the important parameters to describe the land surface characteristics in the urban climates (Coutts et al., 2007). First, the seasonal trends of simulated climate variables and surface-energy budgets for different climate zones were analyzed, as shown in Fig. 4. A higher temperature was observed from June to August, with a distinct pattern in the arid, continental, and temperate climate, where a summer season occurs. For all climate zones,  $T_s$  was considerably higher, in a range of 26.15 °C to 35.60 °C, compared to  $T_a$  (Figs. 4a-d).  $T_s$  values are likely to be more extreme compared to  $T_a$  values because the temperature of the surface is determined by energy flows, which are closely related to the incoming shortwave and outgoing longwave radiation balance. Sensible heat was also higher in all climates, with peak observations during the summer. In arid and tropical climates, H accounted for high proportions during the dry period, ranging from 90.33 W m<sup>-2</sup> to 108.48 W m<sup>-2</sup>, respectively (Fig. 4a, d). On the other hand, arid showed relatively high H and low LE during the summer which might due to the extremely hot summer temperature in the Phoenix, hence decreased the LE. During the winter (December to February), the continental climate recorded negative temperatures of -10.93 °C and -12.43 °C for  $T_a$  and  $T_s$ , respectively (Fig. 4b). In contrast, temperate and tropical climates experienced insignificant changes in temperature ( $T_a$  and  $T_s$ ) due to the hot and humid characteristics of Houston (temperate) and wet and dry conditions of Miami (tropical) all years (Fig. 4c and d).

Fig. 5 depicts the annual variation in climate and energy flux for the arid, continental, temperate, and tropical zones from 1990 to 2014. The tropical city recorded the highest average annual magnitude of the  $T_a$  ( $T_s$ ), at 25.73 °C (27.48 °C), followed by the temperate city, at 21.81 °C (22.65 °C) (Fig. 5a, b). This may be due to the tropical climate's two distinct seasons of wet and dry, lack of significant temperature changes throughout the year, and no marked winter season (Mohammad Harmay & Choi, 2021a). Meanwhile, the continental climate recorded the lowest annual average temperatures of 10.55 °C and 11.33 °C for  $T_a$  and  $T_s$ , respectively (Fig. 5a, b). Minneapolis, which represented the continental climate in this study, experienced greater annual temperature variations due to hot summer and cold winter climate characteristics thus recorded the lowest average annual temperature. Additionally, the greater part of Minneapolis that had the highest vegetative cover surrounding the city, demonstrated lower annual temperatures (Mbuh et al., 2021). Overall, the CLM simulation captured the annual variations in detail, with higher  $T_s$  compared to  $T_a$ , confirming previous climate model simulations (Zhao et al., 2018). The tropical climate city recorded the highest annual values for H and LE, at 100.50 W m<sup>-2</sup> and 59.48 W m<sup>-2</sup>, respectively, compared with its arid, continental, and temperate counterparts (Figs. 5c, d). Warmer ocean water that is heated in the tropics transfer the sensible heat poleward, where the warmer winds that transmit the

sensible heat may also converted the excess heat into the latent heat, due to the evaporation and precipitation (Shaw & Pauluis, 2012). Overall, due to the characteristics of the selected sites of the urban areas, the value of H is higher compared to LE for all climate zones with respect to higher solar absorption, thermal capacity, and lower albedo (Kaloustian & Diab, 2015; Martin et al., 2015).

#### 4.3. Urban warming and the heat-stress index in relation to seasonal climate variability

Fig. 6 describes the average urban temperature warming and heat-stress index as measured by  $T_{urban}$  and  $HI_{urban}$ , respectively, which were obtained from CLM5.0 simulations of the summer, winter, and annual periods. The results demonstrated that  $T_{urban}$  and  $HI_{urban}$  differed based on climate conditions and seasonal dynamics, with significant variations during the winter and annual periods. Overall, higher  $T_{urban}$  and  $HI_{urban}$  values were observed in all cities during the summer compared to the winter season. These results indicate that the warming effects during winter that influence  $T_{urban}$  and  $HI_{urban}$  are not as apparent compared with those of the summer simulation.

The tropical climate recorded the highest summer  $T_{urban}$ , with an average of 33.46 °C for 1990–2014, while the lowest summer urban warming was observed in the temperate climate city, at 29.06 °C (Figs. 6a). Additionally, tropical Miami also recorded the highest winter  $T_{urban}$ , at 23.43 °C, due to the highest  $T_a$  and  $T_s$  in the winter, at 18.22 °C and 19.71 °C, respectively (Fig. 7a and b). This outcome was expected due to the influence of the tropical climate, with only dry and wet seasons that are more prone to relatively high urban overheating, even during the winter (Chakraborty et al., 2020). Furthermore, higher urban warming affected tropical cities which are located in the low-latitude compared to the mid-latitude cities (Chew et al., 2021). This is because, tropics are more exposed to the direct sunlight, hence stored more solar radiation and further increased the urban temperature effect. Besides, Fig. 7c also showed that the sensible heat fluxes for arid and tropical climates peaked, at 108.48 W m<sup>-2</sup> and 108.37 W m<sup>-2</sup>, respectively, during the summer. These results indicate that high sensible heat in the cities may enhancing the UHI effect, particularly in the hot and dry climates.

For the heat-stress index, the summer season also experienced higher values compared to winter and annual  $HI_{urban}$  variations (Fig. 6d-f). The highest summer  $HI_{urban}$  was recorded in the hot climates (arid, temperate, and tropical), compared with the cool climate (continental). Temperate and tropical climates experienced the highest heat stress, at 33.73 °C and 34.44 °C respectively, both of which fall under the “extreme caution” heat-stress category (Fig. 6d). According to the NWS, the heat-stress index is closely related to the effect of humidity and the actual air temperature, which agrees with our findings of relatively high  $T_a$  and lower RH values during the summer in the tropical climate (Fig. 7a and e). However, temperate climate demonstrated different variations of  $T_a$  and RH which are possibly affected by other urban vulnerability factors. Previous study suggested that the heat exposure variables in Houston can be better explained by daily minimum temperature, which is coincident with the heat mortality index (Heaton et al., 2014). The heat hazard in the North American temperate climate was also resulted from the short-term climate events (e.g., heat waves) that vary in daily scale, which lead to some variances in the accumulated seasonal temperatures (Lee et al., 2022). However, the influence of the sensible heat component on the  $HI_{urban}$  are unclear due to variations in the temperate and tropical cities (Fig. 7c), similar with previous research that found some limitations in the heat stress estimation due to the absence of radiation component (Oleson et al., 2015). Generally, the lowest summer  $HI_{urban}$  was observed in the continental climate, which can be considered part of the “caution” range of 27.00 °C to 32.00 °C. Meanwhile, for the annual  $HI_{urban}$ , the temperate and tropical climates showed a similar pattern of 25.06 °C and 27.37 °C, respectively (Fig. 6f).

Overall, the tropical climate city experienced higher urban warming

temperatures, as indicated by  $T_{\text{urban}}$ . These occurrences were also correlated with high sensible heat, which is dominant in the hotter urban areas. The urban heat-stress index also revealed that higher temperatures were recorded in the hot climate cities compared with the cool climate cities. Specifically, the temperate and tropical climate featured notably high  $\Delta\text{HI}_{\text{urban}}$  values that reached the “extreme caution” level, which can cause heat stroke, heat cramps, and heat exhaustion due to prolonged exposure to outdoor activities.

#### 4.4. Long-term trends in urban-rural temperatures and heat stress index

In this section, distinct differences in urban-rural temperatures and the heat-stress index between different climate zones, represented by the UHI effect and  $\Delta\text{HI}$ , respectively, were analyzed. Two different periods were distinguished to determine the effect of urban expansion on the UHI effect and  $\Delta\text{HI}$ . Fig. 8 depicts the annual temporal variability and UHI trends ( $^{\circ}\text{C year}^{-1}$ ) at four different study sites and their average trends for 1990–2000 (first period), 2001–2014 (second period), and 1990–2014 (complete period).

For the arid climate, positive UHI trends of  $0.001\text{ }^{\circ}\text{C year}^{-1}$ ,  $0.007\text{ }^{\circ}\text{C year}^{-1}$ , and  $0.003\text{ }^{\circ}\text{C year}^{-1}$  were reported for the first, second, and complete period, respectively (Fig. 8e). During the second period from 2001 to 2014, the highest annual UHI trend of  $0.007\text{ }^{\circ}\text{C year}^{-1}$  was observed due to the greater fraction of impervious surfaces in Phoenix, along with its hot and dry environment in the arid climate (Fig. 2e). Our

analysis suggests that surfaces with low natural vegetative coverage are characterized by higher longwave emissivity, leading to an increase in the UHI trend (Fischer et al., 2012). In contrast,  $\Delta\text{HI}$  in the arid city exhibited a decreasing trend, with the lowest value recorded during the first period, at  $-0.004\text{ }^{\circ}\text{C year}^{-1}$ . The analysis revealed that  $\Delta\text{HI}$  in the arid climate gradually decreased in 1999, before fluctuating again in 2000 (Fig. 9a). Phoenix, which has an arid desert climate with extremely hot and dry summers, experienced the occasional monsoon and wind shifts that drew moisture northward, resulting in contrasting trends in heat stress (Oleson et al., 2015). Previous study also found that the UHI trend is usually influenced by the urban form process and urban density, while heat stress depends on exposure to the heat of the population (Lemonus et al., 2015).

For the continental climate, the UHI effect followed a decreasing trend, with an annual rate of change of  $-0.006\text{ }^{\circ}\text{C}$  for the 25 years (Fig. 8f). Despite this trend, the continental climate experienced the significant variations in maximum, mean, and minimum UHI effects during this period of  $1.90\text{ }^{\circ}\text{C}$  to  $2.60\text{ }^{\circ}\text{C}$ ,  $0.34\text{ }^{\circ}\text{C}$  to  $0.62\text{ }^{\circ}\text{C}$ , and  $-0.03\text{ }^{\circ}\text{C}$  to  $-0.90\text{ }^{\circ}\text{C}$ , respectively (Fig. 8b). The continental climate, which is characterized by a primarily warm and humid environment, is more sensitive to accelerated regional warming due to summer and winter influences, which reflects the fluctuation in the UHI effect (Esau et al., 2019). Besides, the anthropogenic heat trapping mechanism has been identified as the driving mechanism of the temperature anomalies in the continental climates (Miles & Esau, 2020). The long-term trend in  $\Delta\text{HI}$

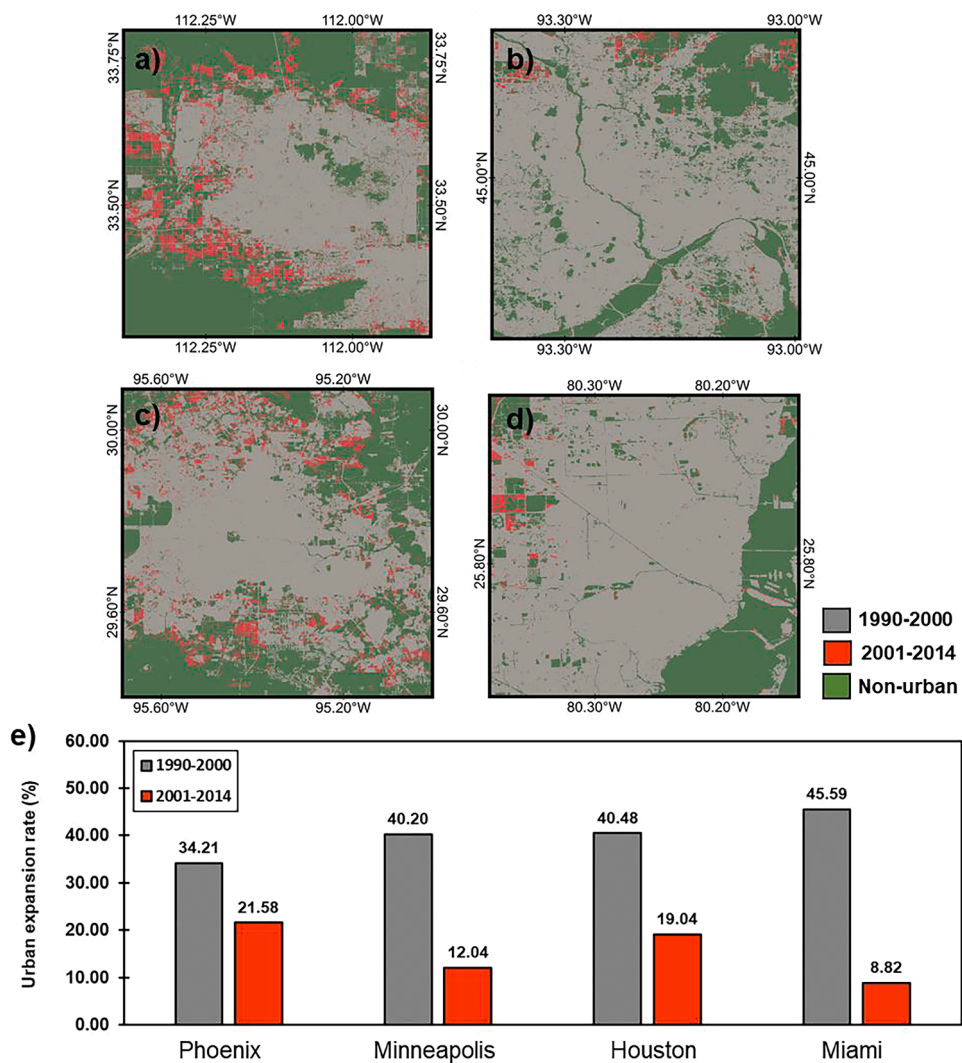
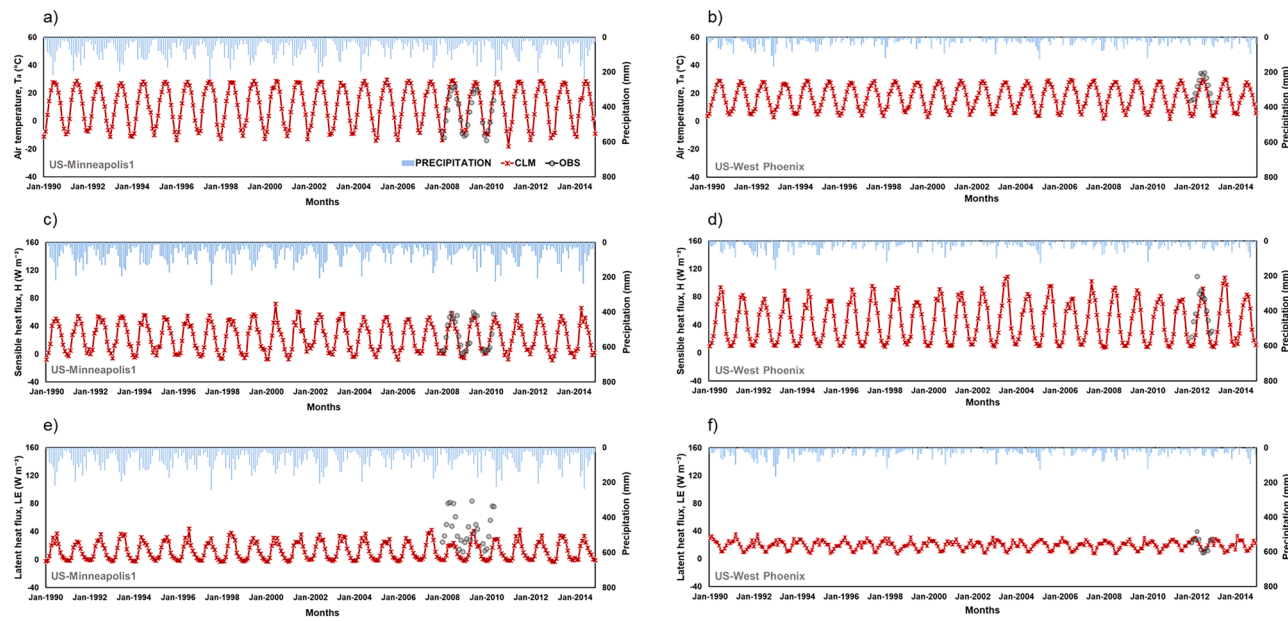
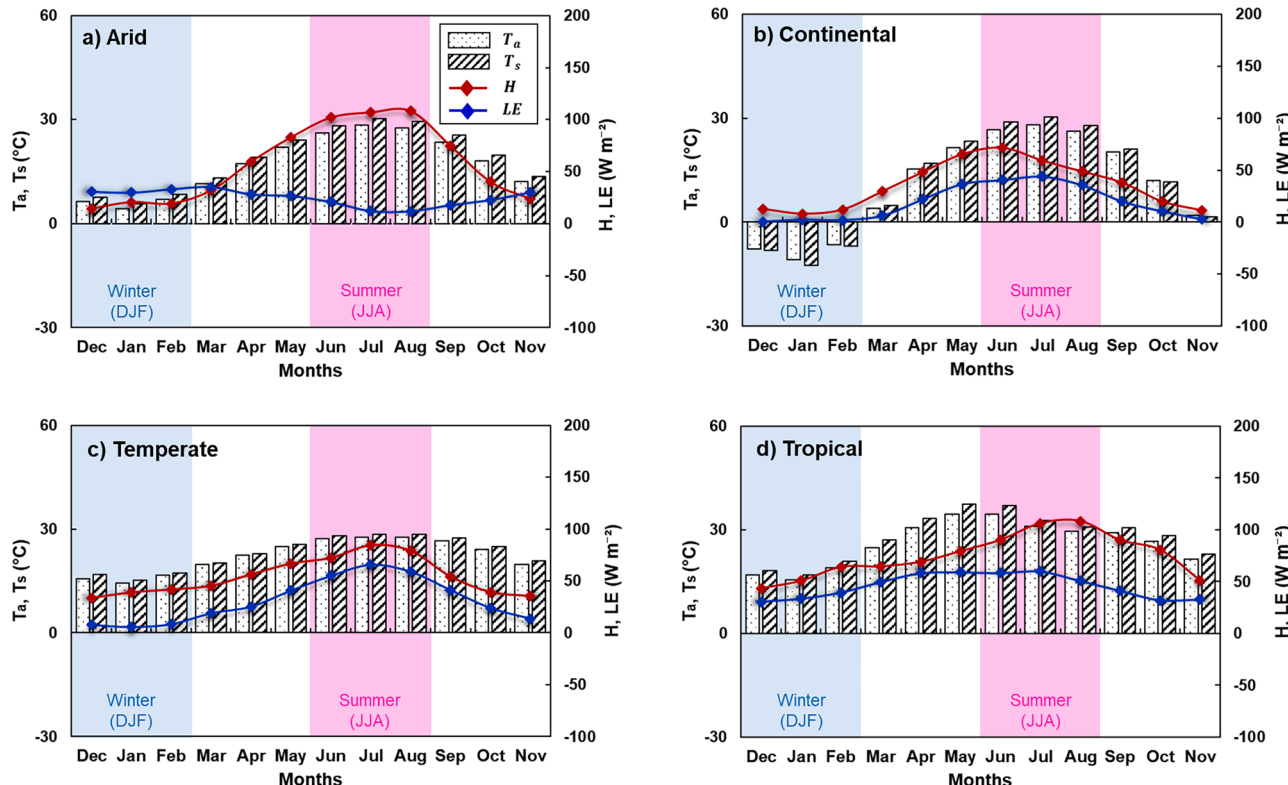


Fig. 2. Spatial pattern of urban extent in a) Phoenix, b) Minneapolis, c) Houston, d) Miami, and e) urban expansion, 1990–2000 and 2001–2014.



**Fig. 3.** Time series of air temperature ( $T_a$ ), sensible heat flux ( $H$ ), and latent heat flux ( $LE$ ) between the CLM simulation and flux tower observations at US-Minneapolis (a–c) and US-West Phoenix (d–f), with precipitation.



**Fig. 4.** Monthly average air temperature ( $T_a$ ), surface temperature ( $T_s$ ), sensible heat flux ( $H$ ), and latent heat flux ( $LE$ ) from 1990 to 2014 for a) arid, b) continental, c) temperate, and d) tropical climate zones. Vertical blue bands indicate winter months (December, January, and February) and vertical magenta bands indicate summer months (June, July, and August).

also supported the UHI pattern, in which a significant increment in the ΔHI trend was observed in the continental climate, with the largest annual changes observed in 2001–2014 ( $0.006 \text{ }^{\circ}\text{C year}^{-1}$ , Fig. 9f).

Houston, which has a temperate climate, experienced an increasing trend in the UHI effect, with the largest change occurring during the second period (2001–2014), at  $0.007 \text{ }^{\circ}\text{C year}^{-1}$ , (Fig. 8g). Houston city

which is located near the coast, is highly influenced by sea breezes and coastal winds, making it sensitive to heat events and the UHI effects (Ramamurthy & Sangobanwo, 2016). Variations in the urban-rural heat-stress index in the temperate climate also followed an annual increasing trend during the first, second, and complete periods, at  $0.002 \text{ }^{\circ}\text{C year}^{-1}$ ,  $0.003 \text{ }^{\circ}\text{C year}^{-1}$ , and  $0.007 \text{ }^{\circ}\text{C year}^{-1}$ , respectively

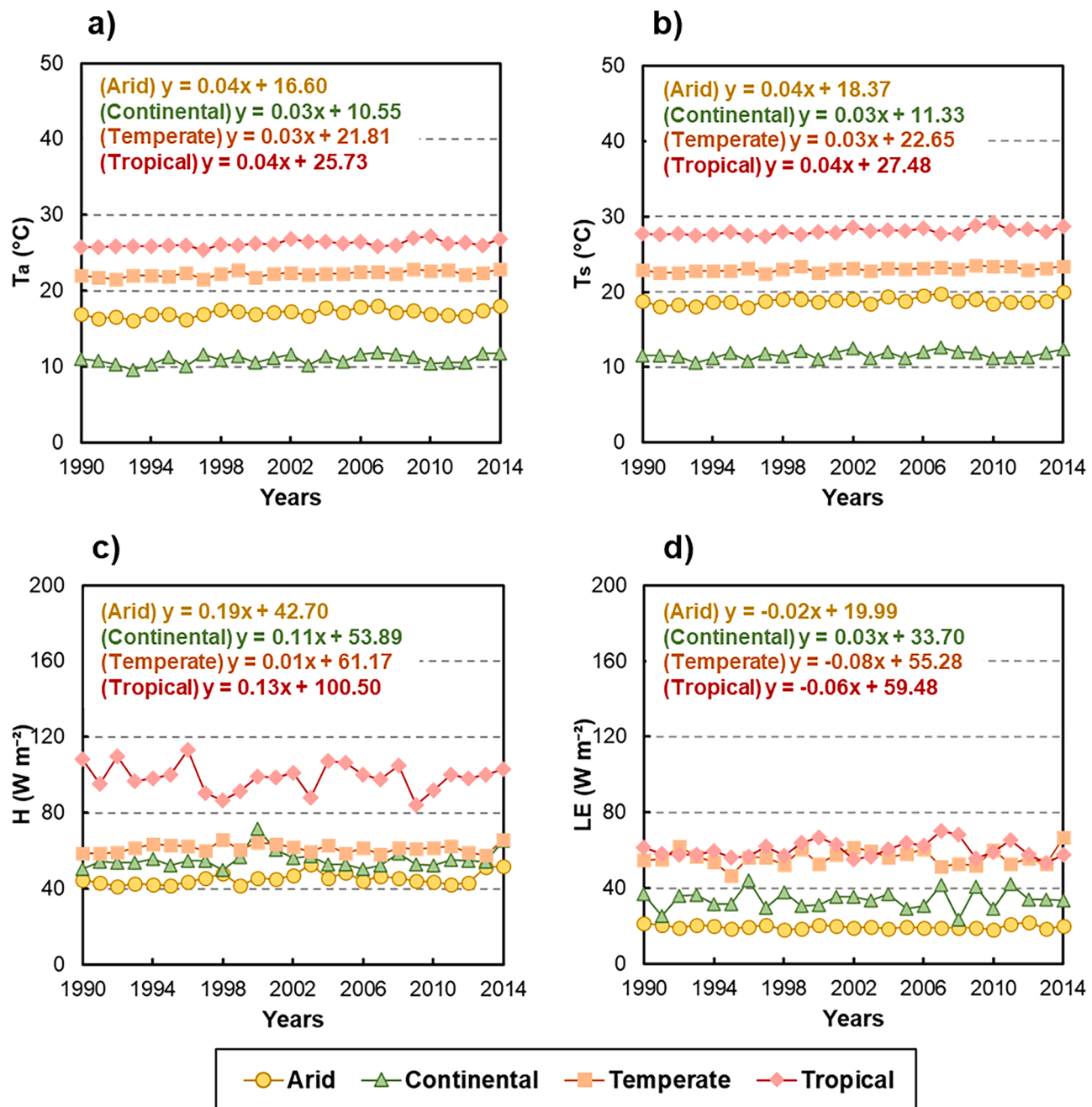


**Fig. 5.** Time series of air temperature ( $T_a$ ), surface temperature ( $T_s$ ), sensible heat flux (H), and latent heat flux (LE) for arid, continental, temperate, and tropical cities from 1990 to 2014.

(Fig. 9g). The temperate climate, which is characterized by hot and humid conditions with hot summertime, is exposed to urban warming and greater heat stress. The combined effects of climate characteristics and land cover changes in Houston with relatively high urban expansion rate of 19.04%, may potentially expose this city towards extreme heat change (Fig. 2e). Conlon et al. (2016) also found that higher urban development has increased the present and future heat exposure of the Houston area. These results are consistent with those of a previous study that found higher urban warming in the cities with lower wind speeds and clear skies (Santamouris, 2016).

For the tropical climate, though the average annual UHI was relatively high with  $2.00\ ^{\circ}\text{C}$  intensity, the UHI trend was found to be decreased annually at  $-0.005\ ^{\circ}\text{C year}^{-1}$  to  $-0.002\ ^{\circ}\text{C year}^{-1}$  (Fig. 8h). This trend may have resulted from the higher amount of heat retention

in the urban substrates that caused lesser heat flux variability thus subsequently led to the smaller temperature range, mainly in the tropical city. Higher soil moisture in the rural surface cover might also mitigate the nocturnal rural cooling and resulting in a weak summer UHI trend, consistent with previous UHI study in Miami (Kedzuf et al., 2011). The annual  $\Delta\text{HI}$  trend was also found to have decreased in the tropical climate, possibly due to an urban-rural soil moisture deficit that was not significantly altered during periods of higher heat stress, which is consistent with findings reported by Chew et al. (2021).

Overall, in terms of the UHI effect, the arid and temperate climates exhibited positive increasing trends during the first, second, and complete periods. The latest period of 2001–2014 showed a relatively high UHI trend of  $0.007\ ^{\circ}\text{C year}^{-1}$ . For  $\Delta\text{HI}$ , the continental and temperate climates exhibited positive annual trends compared with the arid and

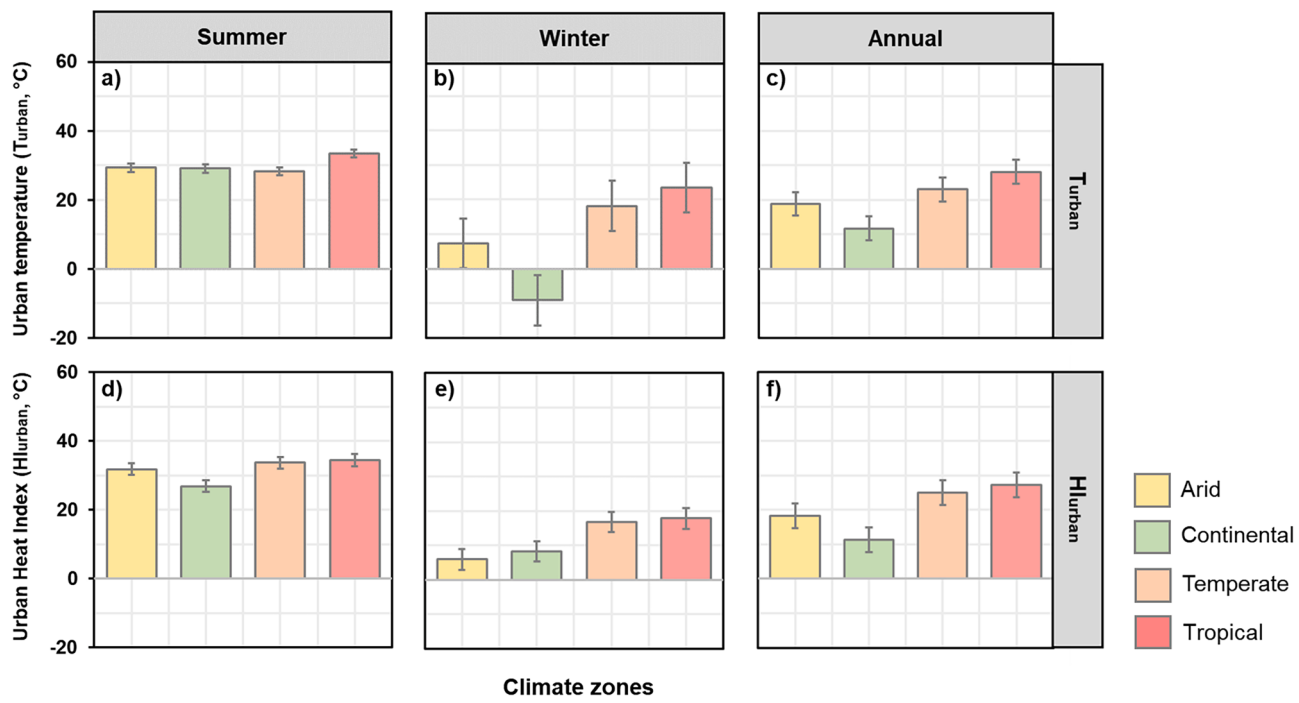


**Fig. 6.** Average seasonal variations of urban temperature ( $T_{\text{urban}}$ ) (a–c) and urban heat index ( $\text{HI}_{\text{urban}}$ ) (d–f) for each climate zone during the summer and winter and annually.

tropical zones. These trends in both the UHI effect and  $\Delta\text{HI}$  can be attributed to climate characteristics and meteorological factors, which will be discussed in the next section.

#### 4.4.1. Characteristics of the UHI effect and heat stress index under different climate and urban dynamics

Table 3 shows the partial correlation between the UHI effect and  $\Delta\text{HI}$  as measured by  $T_a$ ,  $T_s$ , H, LE, RH, and precipitation in the four different climates during the first period (1990–2000), second period (2001–2014), and complete period (1990–2014). In the arid climate, the UHI was negatively (positively) correlated with  $T_a$  and  $T_s$  at  $-0.49$  and  $-0.48$  ( $0.60$  and  $0.64$ ) during the first (second) period. Phoenix city which is dominated by short type vegetation of sagebrushes and grasses in the adjacent rural areas has weakens the temperature contrast between urban and rural, thus led to the negative  $\Delta T$ . Higher aerodynamic resistance that comes from the short-vegetated component compared to its urban landscape has caused the UHI cooling effect, which was found as an evidence of the ‘urban heat sink’ that usually occurred in the arid and desert ecosystem (Imhoff et al., 2010; Zhao et al., 2014). Our analysis also showed that Phoenix had the lowest urban expansion rate of  $34.21\%$  during the first period compared to other cities, along with the highest non-urban coverage, which may also elevate the rural warming effects compared to its adjacent urban side (Fig. 2a and e). Meanwhile, a positive correlation between UHI and temperatures during the second period was supported by higher urban expansion rate of  $21.58\%$  as shown in Fig. 2e, which also coincided with a high increasing UHI trend from 2001 to 2014 ( $0.007\text{ }^{\circ}\text{C year}^{-1}$ , Fig. 8e). Higher impervious surface coverage in the city enhanced the urban temperature warming, leading to a greater UHI intensity. During the complete period (1990–2014), a significant positive correlation between UHI and H was found in the Phoenix, with a statistically significant  $p$ -value of  $< 0.05$ . This was possibly associated with the temperature increase and warmer surfaces that resulted in an increase in longwave radiation emitted from the land surface to the atmosphere, leading to a higher H magnitude (Coutts et al., 2007). High sensible heat flux was also modulated evapotranspiration losses in arid urban areas, thus making the surface more hotter (Templeton et al., 2018). Meanwhile, for  $\Delta\text{HI}$  in the arid

city, the first period (total period) exhibited positive correlations with  $T_a$  and  $T_s$  of  $0.79$  ( $0.67$ ) and  $0.77$  ( $0.68$ ), respectively, with  $p < 0.01$  (Fig. 9a). During the first period,  $\Delta\text{HI}$  experienced a negative trend of  $-0.04\text{ }^{\circ}\text{C decade}^{-1}$  (Fig. 8a), which indicates that the  $T_a$  and  $T_s$  for 1990–2000 mitigated the  $\Delta\text{HI}$  in the arid climate. Due to the limited water available in arid climates, vegetated coverage played a significant role in water storage and evaporation compared with bare soil. Water retention in the vegetation was greater than in urban surfaces and consequently reduced the temperature and heat-stress effects in Phoenix (Fritia et al., 2019).

In the continental climate, the UHI effect correlated somewhat with precipitation ( $0.49$ ,  $p < 0.05$ ; Table 3) for 1990–2000. These conditions may be due to the characteristics of continental climates, which experience frequent precipitation over the year, along with a relatively low urban expansion rate of  $12.04\%$  in the continental city (Fig. 2b and e). Previous research conducted by the U.S National Aeronautics and Space Administration in 2006 concluded that the destabilized urban atmospheric air which created rain-producing clouds and abundant precipitation, could initiate the UHI effect. Brook (2015) also argued that UHI was positively correlated with precipitation events due to the unstable atmospheric conditions. The UHI-thermal forcing was also found to be clearly noticeable with the presence of rainfall anomalies in Minneapolis that lies in the Central Plains of the U.S. which was primarily associated with higher convection efficiency, as described by Ganeshan et al. (2013). In contrast, LE demonstrated a negative correlation with UHI for 1990–2014 of  $-0.35$ , with a  $p < 0.05$ . These contrast relationship for precipitation and latent heat revealed that the latent heating mechanism from precipitation does not produce dominant warm raining process in Minneapolis. Our results were also supported by previous study which stated that warmer rain fractions that yields latent heat are lesser in mid latitudes and polar regions, whereas these areas are more dominated by the cold precipitation with lesser latent heating contributions (Nelson & L'Ecuyer, 2018). Besides, the negative trend between UHI and H explained that UHI was exacerbated due to lower background sensible heat from lesser incoming short radiation received in the city that is located away from the equator (Varquez & Kanda, 2018). On the other hand, air and surface temperatures were positively correlated with  $\Delta\text{HI}$ ,

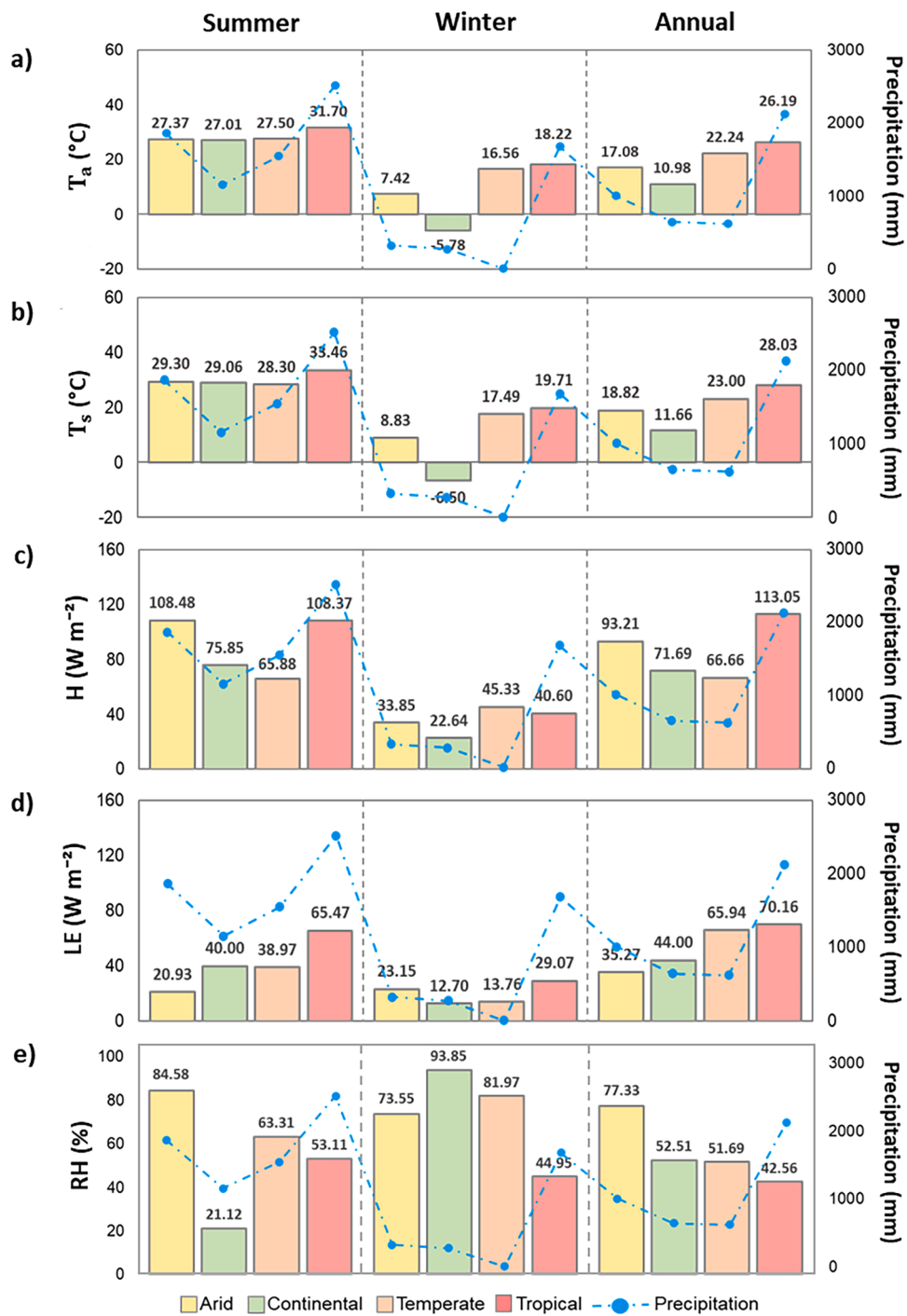


**Fig. 7.** Average seasonal variations of a) air temperature ( $T_a$ ), b) surface temperature ( $T_s$ ), c) relative humidity (RH), sensible heat flux ( $H$ ), and d) latent heat flux (LE) for each climate zone during the summer, winter, and annually, with precipitation.

with the strongest correlation (1990–2000) for  $T_a$  ( $T_s$ ) of 1.00 (0.77) ( $p < 0.01$ ; Table 3), but correlated negatively with humidity. Previous research have found that the heat-stress extremes coincided closely with humidity rather than temperature; however this evidence was stronger in warmer regions (Raymond et al., 2017). In the present study, a strong positive (negative) correlation with temperature (humidity) indicates that temperature and humidity had adverse effects on heat-stress factors in the continental climate.

For the temperate climate, the UHI was significantly correlated with  $T_a$  and  $T_s$  over the last 15 years of the study period (2001–2014), with respective statistical correlations of 0.56 and 0.68 ( $p < 0.01$ , Table 3).

During these periods, the urbanization rate of Houston increased, with a relatively high urban expansion rate of 19.04% (Fig. 2e), and was concentrated in the same area, as shown in Fig. 2c. The conversion of naturally vegetated surfaces into urban and built-up areas increased temperature warming, leading to a more intense UHI. These occurrences also affected the UHI trend, with a positive trend evident throughout 2001 to 2014 ( $0.007\text{ }^{\circ}\text{C year}^{-1}$ , Fig. 8a). The  $\Delta\text{HI}$  was also positively correlated with  $T_a$  and  $T_s$ , which indicates that an increase in temperature may further increase the heat-stress index, particularly for  $T_a$  during 1990–2000 (1990–2014), with a 0.82 (0.79) statistical correlation ( $p < 0.01$ ; Table 3).

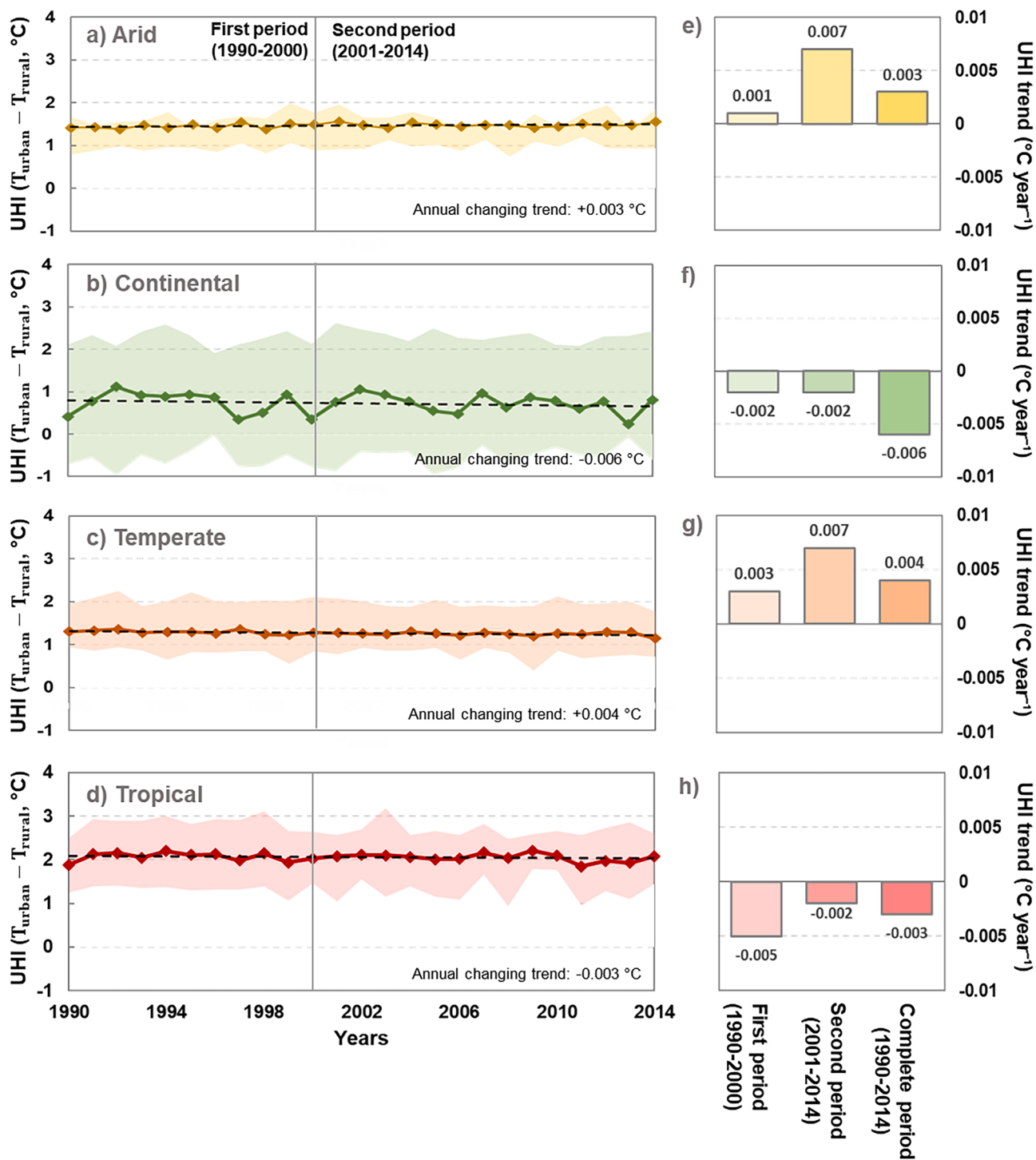


**Fig. 8.** Temporal variability in annual urban heat island (UHI) intensities ( $T_{\text{urban}} - T_{\text{rural}}$ ) from 1990 to 2014 in arid, continental, temperate, and continental cities (a-d) with the UHI trend for the first period (1990–2000), second period (2001–2014), and complete period (1990–2014) (e-h). Bold lines represent mean values, while shaded regions represent the range of maximum and minimum values for each year.

Due to the climate conditions in the tropical city, RH in Miami was negatively correlated with the UHI effect but positively correlated with  $\Delta\text{HI}$  ( $p < 0.01$ ; Table 3). The results indicated that, as the humidity decreased, it will also increase the UHI effect in the tropical city. This condition can be characterized when the high urban temperature from the urbanization process will lead to a decrease in relative humidity and drier air, thus, increases the UHI effect; equivalent to the high urbanization rate of 45.59% in the earliest period (Fig. 2e). This relationship between RH and UHI is supported by a previous results by Luo et al.

(2022) who found that lower RH was associated with a significant UHI effect in the tropical Pearl River Delta urban agglomeration. Roth (2007) also agreed that the thermal properties associated with moisture availability of rural reference is an important factor affecting the UHI in tropical climates.  $\Delta\text{HI}$  was also significantly correlated with  $T_a$  and  $T_s$ , particularly for 1990–2014, with statistical correlations of 0.51 and 0.57, respectively ( $p < 0.01$ ; Table 3). In recent work, these conditions showed that  $\Delta\text{HI}$  in tropical climate coincided significantly with temperature and humidity, consistent with those of Oleson et al. (2015).

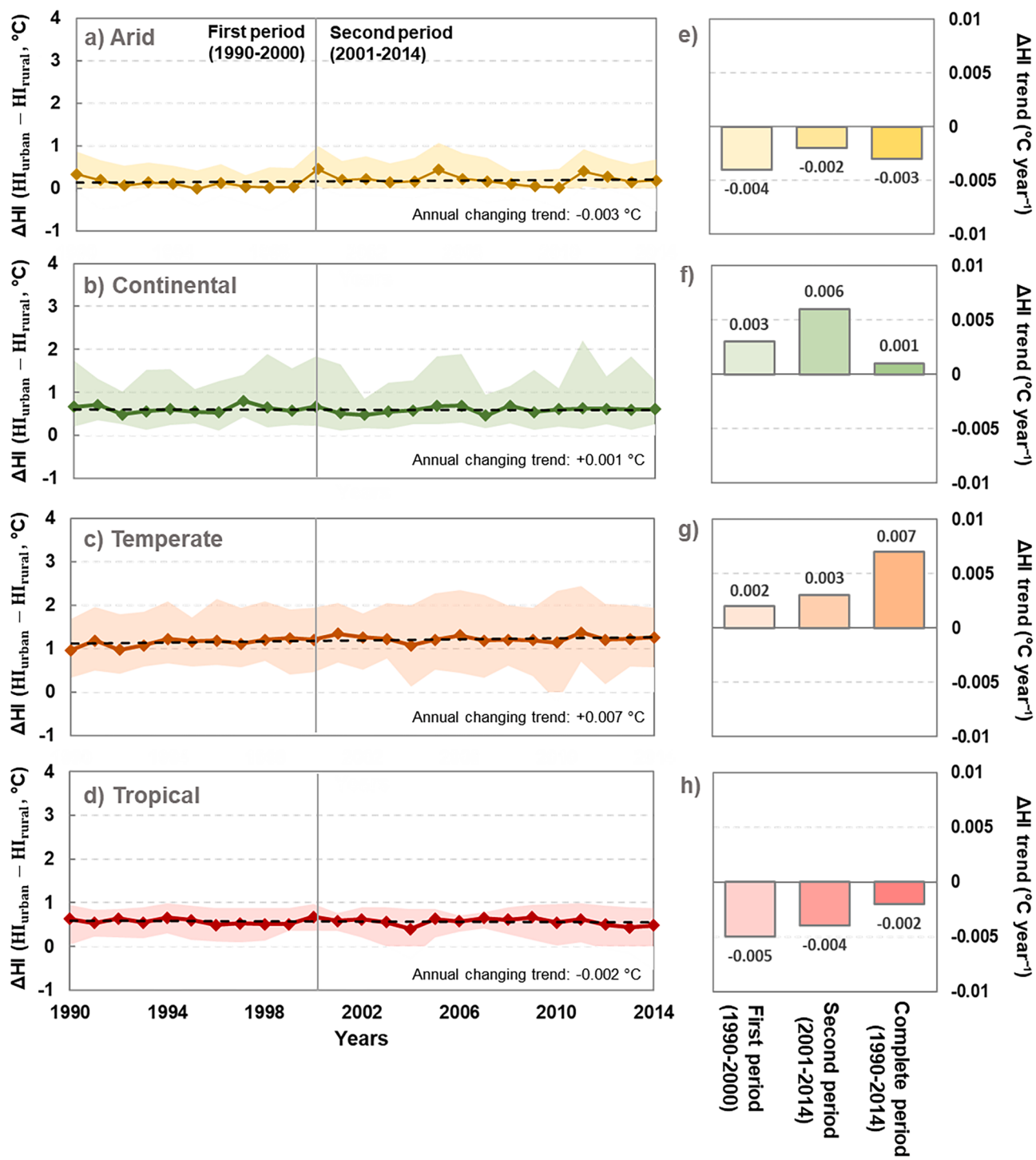


**Fig. 9.** Temporal variability in annual change in the heat index,  $\Delta\text{HI}$  ( $\text{HI}_{\text{urban}} - \text{HI}_{\text{rural}}$ ,  $^{\circ}\text{C}$ ), from 1990 to 2014 in arid, continental, temperate, and continental cities (a-d) with  $\Delta\text{HI}$  trends for first period (1990–2000), second period (2001–2014), and complete period (1990–2014) (e-h). Bold lines represent the mean values, while the shaded regions represent the range of maximum and minimum values for each year.

Besides, previous modeling studies also concluded that the urban convection area which often located near the coastal and equatorial regions exacerbated a high heat-stress environment due to the combined effect from temperature and humidity partitioning (Buzan et al., 2015; Fischer & Knutti, 2013).

Generally, each climate zone exhibited different influences of climate parameters and urban dynamics on the UHI and  $\Delta\text{HI}$ . The UHI effect was positively correlated with  $T_a$  and  $T_s$  in hotter climates (arid and temperate) (Table 3). Meanwhile, in the continental climate zone,

precipitation could be a main driver influencing the UHI effect. For  $\Delta\text{HI}$ , all climate zones showed a positive correlation with  $T_a$  and  $T_s$ , and with RH for the tropical climate. The relationship between the UHI effect and  $\Delta\text{HI}$  with hydrometeorological parameters was also influenced by different urbanization rate during the first period (1990–2000) and the second period (2001–2014) in each city.

**Table 3**

Partial correlation between urban heat island (UHI) and urban-rural differences of heat index ( $\Delta$ HI) with air temperature ( $T_a$ ), surface temperature ( $T_s$ ), sensible heat flux (H), latent heat flux (LE), relative humidity (RH), and precipitation. Note: \*\*correlation is significant at 0.01 level; \*correlation is significant at 0.05 level.

			$T_a$	$T_s$	H	LE	RH	Precipitation
Arid	UHI	1990–2000	*−0.49	*−0.48	0.44	0.24	0.06	0.46
		2001–2014	**0.60	**0.64	−0.03	−0.08	0.12	0.12
		1990–2014	*0.32	*0.33	*0.28	0.07	−0.01	−0.07
	$\Delta$ HI	1990–2000	**0.79	**0.77	−0.26	0.24	−0.16	−0.13
		2001–2014	*−0.52	*−0.51	0.25	−0.10	−0.12	−0.34
		1990–2014	**0.67	**0.68	−0.15	0.21	−0.09	−0.06
Continental	UHI	1990–2000	0.27	0.22	0.09	−0.35	−0.31	*0.49
		2001–2014	0.09	−0.08	*−0.41	−0.36	0.03	−0.06
		1990–2014	0.06	−0.06	−0.21	*−0.35	−0.05	0.06
	$\Delta$ HI	1990–2000	**1.00	**0.77	0.02	−0.42	−0.53	0.35
		2001–2014	**0.93	**0.69	0.01	0.06	*−0.52	−0.34
		1990–2014	**0.94	**0.71	−0.03	−0.12	*−0.46	0.10
Temperate	UHI	1990–2000	0.46	−0.37	−0.20	0.38	0.20	−0.09
		2001–2014	**0.56	**0.68	−0.01	0.19	0.12	−0.01
		1990–2014	0.49	0.59	−0.05	0.21	0.13	−0.05
	$\Delta$ HI	1990–2000	**0.82	**0.70	−0.16	0.35	0.09	0.31
		2001–2014	0.10	0.03	0.08	0.36	−0.23	−0.19
		1990–2014	**0.79	**0.71	0.07	0.08	*−0.31	−0.01
Tropical	UHI	1990–2000	0.16	−0.02	−0.38	0.42	*−0.67	0.09
		2001–2014	0.17	−0.01	0.10	0.12	*−0.60	−0.21
		1990–2014	−0.03	−0.15	−0.09	0.13	*−0.63	−0.02
	$\Delta$ HI	1990–2000	0.35	0.24	0.09	−0.27	*0.68	−0.09
		2001–2014	0.39	**0.56	−0.30	−0.45	0.36	−0.21
		1990–2014	**0.51	**0.57	−0.12	−0.21	**0.53	−0.06

## 5. Conclusion

In the present study, the UHI effect and thermal heat-stress index of Phoenix, Minneapolis, Houston, and Miami, which represented arid, continental, temperate, and tropical climate zones, were analyzed. A CLM5.0 simulation was conducted to quantify the climate and surface-energy flux parameters, along with the UHI effect and HI from 1990 to 2014. Generally, our results showed that the model had a high simulation accuracy when compared with the flux towers data. The city in the tropical climate had the highest  $T_{\text{urban}}$ , which was correlated with a relatively high H in the lower latitudes, which receive more direct sunlight as they are near the equator. The HI<sub>urban</sub> observed in the temperate and tropical climates reached the “extreme caution” level of between 33.00 °C and 39.00 °C, during which heat stroke, heat cramps, and heat exhaustion can be anticipated, according to the NWS. Our study found that urban-rural temperature differences are higher compared to heat stress, with respective ranges of 0.73 °C to 2.07 °C and 0.14 °C to 1.23 °C. In terms of the annual trends, arid and temperate climates showed a positive increasing trend in the UHI effect during 2001–2014 due to high urban expansion rates of 21.58% and 19.04%, respectively. In contrast, continental and temperate climates experienced an increasing trend in  $\Delta$ HI due to the accelerated regional warming effects of the warm and humid and the hot and humid environments, respectively. We found that the UHI effect has a positive relationship with  $T_a$  and  $T_s$  in the hotter climates, while precipitation has more influences in the continental climate along with the lower urbanization rate. For  $\Delta$ HI,  $T_a$  and  $T_s$  were positively correlated in all climate zones.

Overall, our results provide notable insights for the urban climate dynamics by integrating a climate model simulation with quantification of climate and surface-energy flux parameters, along with the urban phenomena of the UHI effect and HI. Our findings shed light on the way UHI trends and HI interact with climate and energy fluxes in the urban areas, by incorporating the climate model of CLM5.0. The model simulation can be utilized to provide information for urban climate mitigation impacts and reduce heat exposure for cities' population. This study also anticipates for the identification of the urban-heat risk areas and the vulnerability of UHI and heat stress, which could be help for the urban mitigation and sustainable urban development. This is because, U.S. continent are highly exposed to the heat mortality and morbidity. For

the future works, more heat stress indices could be employed to consider more heat stress variables and better elucidate the heat hazards for human morbidity and mortality. Besides, since our study only focused on the U.S cities, future studies should also assess other climate regions with different urban densities and building types.

## Declaration of Competing Interest

The authors declare no competing interests.

## Data availability

The data that has been used is confidential.

## Acknowledgements

This research was supported by a grant (2021-MOIS35-003) of ‘Policy-linked Technology Development Program on Natural Disaster Prevention and Mitigation’ funded by Ministry of Interior and Safety (MOIS, Korea). We would like to thank the Central Arizona – Phoenix Long-Term Ecological Research and Arizona State University for kindly providing the flux tower data at Phoenix site. We also acknowledge the Urban-PLUMBER Project and University of California, Santa Barbara for providing the urban flux tower dataset at Minneapolis site.

## References

- Adams, M. P., & Smith, P. L. (2014). A systematic approach to model the influence of the type and density of vegetation cover on urban heat using remote sensing. *Landscape and Urban Planning*, 132(August 2003), 47–54. <https://doi.org/10.1016/j.landurbplan.2014.08.008>
- Andrews, T., Forster, P. M., & Gregory, J. M. (2009). A surface energy perspective on climate change. *Journal of Climate*, 22(10), 2557–2570. <https://doi.org/10.1175/2008JCLI2759.1>
- Arnfield, A. J. (2003). Two decades of urban climate research: A review of turbulence, exchanges of energy and water, and the urban heat island. *International Journal of Climatology*, 23(1), 1–26. <https://doi.org/10.1002/joc.859>
- Baker, L. A., Brazel, A. J., Selover, N., Martin, C., McIntyre, N., Steiner, F. R., Nelson, A., & Musacchio, L. (2002). Urbanization and warming of Phoenix (Arizona, USA): Impacts, feedbacks and mitigation. *Urban Ecosystems*, 6, 183–203.
- Boyd, D., Pathak, M., van Diemen, R., & Skea, J. (2022). Mitigation co-benefits of climate change adaptation: A case-study analysis of eight cities. *Sustainable Cities and Society*, 77(August 2021). <https://doi.org/10.1016/j.scs.2021.103563>

- Brook, T. (2015). Temperature and precipitation extremes. *The Troubled Empire*. <https://doi.org/10.4159/9780674056206-012>
- Buzan, J. R., Oleson, K., & Huber, M. (2015). Implementation and comparison of a suite of heat stress metrics within the Community Land Model version 4.5. *Geoscientific Model Development*, 8(2), 151–170. <https://doi.org/10.5194/gmd-8-151-2015>
- Cao, C., Lee, X., Liu, S., Schultz, N., Xiao, W., Zhang, M., & Zhao, L. (2016). Urban heat islands in China enhanced by haze pollution. *Nature Communications*, 7, 1–7. <https://doi.org/10.1038/ncomms12509>
- Chakraborty, T., Hsu, A., Manya, D., & Sheriff, G. (2020). A spatially explicit surface urban heat island database for the United States: Characterization, uncertainties, and possible applications. *ISPRS Journal of Photogrammetry and Remote Sensing*, 168 (April), 74–88. <https://doi.org/10.1016/j.isprsjprs.2020.07.021>
- Chew, L. W., Liu, X., Li, X. X., & Norford, L. K. (2021). Interaction between heat wave and urban heat island: A case study in a tropical coastal city, Singapore. *Atmospheric Research*, 247(July 2020), Article 105134. <https://doi.org/10.1016/j.atmosres.2020.105134>
- Conlon, K., Monaghan, A., Hayden, M., & Wilhelmi, O. (2016). Potential impacts of future warming and land use changes on intra-urban heat exposure in Houston, Texas. *PLoS One*, 11(2), 1–19. <https://doi.org/10.1371/journal.pone.0148890>
- Conti, S., Meli, P., Minelli, G., Solimini, R., Tocacceli, V., Vichi, M., Beltrano, C., & Perini, L. (2005). Epidemiologic study of mortality during the Summer 2003 heat wave in Italy. *Environmental Research*, 98(3), 390–399. <https://doi.org/10.1016/j.enres.2004.10.009>
- Coutts, A. M., Beringer, J., & Tapper, N. J. (2007). Impact of increasing urban density on local climate: Spatial and temporal variations in the surface energy balance in Melbourne, Australia. *Journal of Applied Meteorology and Climatology*, 46(4), 477–493. <https://doi.org/10.1175/JAM2462.1>
- Dahal, K., Licker, R., Abatzoglou, J. T., & Decler-Barreto, J. (2019). Increased frequency of and population exposure to extreme heat index days in the United States during the 21st century. *Environmental Research Communications*, 1(7). <https://doi.org/10.1088/2515-7620/ab27cf>
- Davis, R. E., Knappenberger, P. C., Michaels, P. J., & Novicoff, W. M. (2003). Changing heat-related mortality in the United States. *Environmental Health Perspectives*, 111 (14), 1712–1718. <https://doi.org/10.1289/ehp.6336>
- Demuzere, M., Oleson, K., Coutts, A. M., Pigeon, G., & van Lipzig, N. P. M. (2013). Simulating the surface energy balance over two contrasting urban environments using the community land model urban. *International Journal of Climatology*, 33(15), 3182–3205. <https://doi.org/10.1002/joc.3656>
- Divya, Y., Gopinathan, P., Jayachandran, K., & Al-Quraishi, A. M. F. (2021). Color slices analysis of land use changes due to urbanization in a city environment of Miami Area, South Florida, USA. *Modeling Earth Systems and Environment*, 7(1), 537–546. <https://doi.org/10.1007/s40808-020-00883-x>
- Edmondson, J. L., Stott, I., Davies, Z. G., Gaston, K. J., & Leake, J. R. (2016). Soil surface temperatures reveal moderation of the urban heat island effect by trees and shrubs. *Scientific Reports*, 6, 1–8. <https://doi.org/10.1038/srep33708>
- Eladesoky, A. H., Gil, J., & Pont, M. B. (2022). Combining environmental and social dimensions in the typomorphological study of urban resilience to heat stress. *Sustainable Cities and Society*, 83(January), Article 103971. <https://doi.org/10.1016/j.scs.2022.103971>
- Emerson, M., Bratter, J., Howel, J., & Wilner, J. (2012). *Houston region grows more racially/ethnically diverse with small declines in segregation - a Joint report analyzing census data from 1990, 2000, and 2010*. Houston, Texas: Kinder Institute for Urban Research, Rice University.
- Esau, I., Miles, V., Varentsov, M., Konstantinov, P., & Melnikov, V. (2019). Spatial structure and temporal variability of a surface urban heat island in cold continental climate. *Theoretical and Applied Climatology*, 137(3–4), 2513–2528. <https://doi.org/10.1007/s00704-018-02754-z>
- Fischer, E. M., & Knutti, R. (2013). Robust projections of combined humidity and temperature extremes. *Nature Climate Change*, 3(2), 126–130. <https://doi.org/10.1038/nclimate1682>
- Fischer, E. M., Oleson, K. W., & Lawrence, D. M. (2012). Contrasting urban and rural heat stress responses to climate change. *Geophysical Research Letters*, 39(3), 1–8. <https://doi.org/10.1029/2011GL050576>
- Fischer, E. M., & Schär, C. (2010). Consistent geographical patterns of changes in high-impact European heatwaves. *Nature Geoscience*, 3(6), 398–403. <https://doi.org/10.1038/ngeo866>
- Fitria, R., Kim, D., Baik, J., & Choi, M. (2019). Impact of biophysical mechanisms on urban heat island associated with climate variation and urban morphology. *Scientific Reports*, 9(1), 1–13. <https://doi.org/10.1038/s41598-019-55847-8>
- Ganesan, M., Murtaguduge, R., & Imhoff, M. L. (2013). A multi-city analysis of the UHI-influence on warm season rainfall. *Urban Climate*, 6, 1–23. <https://doi.org/10.1016/j.uclim.2013.09.004>
- Gedzelman, S. D., Austin, S., Cermak, R., Stefano, N., Partridge, S., Quesenberry, S., & Robinson, D. A. (2003). Mesoscale aspects of the Urban Heat Island around New York City. *Theoretical and Applied Climatology*, 75(1–2), 29–42. <https://doi.org/10.1007/s00704-002-0724-2>
- Golden, J. S., Hartz, D., Brazel, A., Luber, G., & Phelan, P. (2008). A biometeorology study of climate and heat-related morbidity in Phoenix from 2001 to 2006. *International Journal of Biometeorology*, 52(6), 471–480. <https://doi.org/10.1007/s00484-007-0142-3>
- Heaton, M. J., Sain, S. R., Greasby, T. A., Uejio, C. K., Hayden, M. H., Monaghan, A. J., Boehnert, J., Sampson, K., Banerjee, D., Nepal, V., & Wilhelmi, O. V. (2014). Characterizing urban vulnerability to heat stress using a spatially varying coefficient model. *Spatial and Spatio-Temporal Epidemiology*, 8, 23–33. <https://doi.org/10.1016/j.sste.2014.01.002>
- Imhoff, M. L., Zhang, P., Wolfe, R. E., & Bounoua, L. (2010). Remote sensing of the urban heat island effect across biomes in the continental USA. *Remote Sensing of Environment*, 114(3), 504–513. <https://doi.org/10.1016/j.rse.2009.10.008>
- International Energy Agency. (2008). *World energy outlook 2008*. International Energy Agency. <https://doi.org/10.1049/ep.1977.0180>
- Jenerette, D. G., Harlan, S. L., Stefanov, W. L., & Martin, C. A. (2011). Ecosystem services and urban heat landscape moderation: Water, green spaces, and social inequality in Phoenix, USA. *Ecological Applications*, 21(7), 2637–2651. <https://doi.org/10.1890/10-1493.1>
- Jin, M. S. (2012). Developing an index to measure urban heat island effect using satellite land skin temperature and land cover observations. *Journal of Climate*, 25(18), 6193–6201. <https://doi.org/10.1175/JCLI-D-11-00509.1>
- Kaloustian, N., & Diab, Y. (2015). Effects of urbanization on the urban heat island in Beirut. *Urban Climate*, 14, 154–165. <https://doi.org/10.1016/j.uclim.2015.06.004>
- Kedzuf, N. J., Zuidema, P., & Mcnoldy, B. (2011). Seasonal variability and trends of the Miami urban heat island. 1–6.
- Kendall, A. M. G. (1938). A new measure of rank correlation. *Journal of American Statistical Association*, 30(12), 81–89.
- Kenward, A., Yawitz, D., & Sanford, T. (2014). Summer in the city: Hot and getting hotter. *Climate Central*, 1–29.
- Kim, H., Gu, D., & Kim, H. Y. (2018). Effects of Urban Heat Island mitigation in various climate zones in the United States. *Sustainable Cities and Society*, 41(January), 841–852. <https://doi.org/10.1016/j.scs.2018.06.021>
- Kokkonen, T. V., Grimmond, C. S. B., Räty, O., Ward, H. C., Christen, A., Oke, T. R., Kotthaus, S., & Järvi, L. (2018). Sensitivity of Surface Urban Energy and Water Balance Scheme (SUEWS) to downscaling of reanalysis forcing data. *Urban Climate*, 23, 36–52. <https://doi.org/10.1016/j.uclim.2017.05.001>
- Kumar, P., Rai, A., Upadhyaya, A., & Chakraborty, A. (2022). Analysis of heat stress and heat wave in the four metropolitan cities of India in recent period. *Science of the Total Environment*, 818, Article 151788. <https://doi.org/10.1016/j.scitotenv.2021.151788>
- Lawrence, D. M., Oleson, K. W., Flanner, M. G., Fletcher, C. G., Lawrence, P. J., Levis, S., Swenson, S. C., & Bonan, G. B. (2012). The CCSM4 land simulation, 1850–2005: Assessment of surface climate and new capabilities. *Journal of Climate*, 25(7), 2240–2260. <https://doi.org/10.1175/JCLI-D-11-00103.1>
- Lee, S. Y., Lung, S. C. C., Chiu, P. G., Wang, W. C., Tsai, I. C., & Lin, T. H. (2022). Northern hemisphere urban heat stress and associated labor hour hazard from ERA5 reanalysis. *International Journal of Environmental Research and Public Health*, 19(13). <https://doi.org/10.3390/ijerph19138163>
- Lemonsu, A., Viguié, V., Daniel, M., & Masson, V. (2015). Vulnerability to heat waves: Impact of urban expansion scenarios on urban heat island and heat stress in Paris (France). *Urban Climate*, 14, 586–605. <https://doi.org/10.1016/j.uclim.2015.10.007>
- Luo, Z., Liu, J., Shao, W., Zhou, J., & Jia, R. (2022). Distribution of dry and wet islands in the Pearl River Delta urban agglomeration using numerical simulations. *Atmospheric Research*, 273(March), Article 106170. <https://doi.org/10.1016/j.atmosres.2022.106170>
- Mann, B. H. (1945). Nonparametric tests against trend. *Econometrica : Journal of the Econometric Society*, 13(3), 245–259. <http://www.jstor.com/stable/1907187>
- Martin, P., Baudouin, Y., & Gachon, P. (2015). An alternative method to characterize the surface urban heat island. *International Journal of Biometeorology*, 59(7), 849–861. <https://doi.org/10.1007/s00484-014-0902-9>
- Mbuhi, M. J., Wheeler, R., & Cook, A. (2021). Spatiotemporal analysis of urban heat island intensification in the city of Minneapolis-St. Paul and Chicago metropolitan areas using Landsat data from 1984 to 2016. *Geocarto International*, 36(14), 1565–1590. <https://doi.org/10.1080/10106049.2019.1655802>
- McElroy, S., Schwarzbach, L., Green, H., Corcos, I., Guirguis, K., Gershunov, A., & Benmarhnia, T. (2020). Defining heat waves and extreme heat events using sub-regional meteorological data to maximize benefits of early warning systems to population health. *Science of the Total Environment*, 721, Article 137678. <https://doi.org/10.1016/j.scitotenv.2020.137678>
- McMichael, A. J., Woodruff, R. E., & Hales, S. (2006). Climate change and human health: Present and future risks. *Lancet (London, England)*, 367(9513), 859–869. [https://doi.org/10.1016/S0140-6736\(06\)68079-3](https://doi.org/10.1016/S0140-6736(06)68079-3)
- Menzer, O., & McFadden, J. P. (2017). Statistical partitioning of a three-year time series of direct urban net CO<sub>2</sub> flux measurements into biogenic and anthropogenic components. *Atmospheric Environment*, 170, 319–333. <https://doi.org/10.1016/j.atmosenv.2017.09.049>
- Miles, V., & Esau, I. (2020). Surface urban heat islands in 57 cities across different climates in northern Fennoscandia. *Urban Climate*, 31(August 2019), Article 100575. <https://doi.org/10.1016/j.uclim.2019.100575>
- Mirzaei, P. A., & Haghhighat, F. (2010). Approaches to study Urban Heat Island - Abilities and limitations. *Building and Environment*, 45(10), 2192–2201. <https://doi.org/10.1016/j.buildenv.2010.04.001>
- Mohammad Harmay, N. S., & Choi, M. (2021a). Effects of heat waves on urban warming across different urban morphologies and climate zones. *Building and Environment*, 209, 108677. <https://doi.org/10.1016/j.buildenv.2021.108677>
- Mohammad Harmay, N. S., Kim, D., Choi, M. (2021b). Urban Heat Island associated with Land Use / Land Cover and climate variations in Melbourne, Australia. *Sustainable Cities and Society*, 69 (2021b), 102861. doi:10.1016/j.scs.2021.102861.
- Nelson, E. L., & L'Ecuyer, T. S. (2018). Global character of latent heat release in oceanic warm rain systems. *Journal of Geophysical Research: Atmospheres*, 123(10), 4797–4817. <https://doi.org/10.1002/2017JD027844>
- Nematchoua, M. K., Ricciardi, P., Orosa, J. A., & Buratti, C. (2018). A detailed study of climate change and some vulnerabilities in Indian Ocean: A case of Madagascar island. *Sustainable Cities and Society*, 41(February), 886–898. <https://doi.org/10.1016/j.scs.2018.05.040>

- Nguyen, C. T., Chidhaisong, A., Limsakul, A., Varnakovida, P., Ekkawatpanit, C., Diem, P. K., & Diep, N. T. H. (2022). How do disparate urbanization and climate change imprint on urban thermal variations? A comparison between two dynamic cities in Southeast Asia. *Sustainable Cities and Society*, 82(September 2021), Article 103882. <https://doi.org/10.1016/j.scs.2022.103882>
- Oke, T. R. (1973). City size and the Urban Heat Island. *Atmospheric Environment*, 7, 769–779.
- Oke, T. R. (1982). The energetic basis of the urban heat island. *Quarterly Journal of the Royal Meteorological Society*, 108(455), 1–24. <https://doi.org/10.1002/qj.49710845502>
- Oke, T. R., & Cleugh, H. A. (1987). Urban heat storage derived as energy balance residuals. *Boundary-Layer Meteorology*, 39(3), 233–245. <https://doi.org/10.1007/BF00116120>
- Oleson, K. W., & Bonan, G. B. (2010). Technical description of an urban parameterization for the Community Land Model (CLMU). *Tech. Note NCAR, April*. <http://nlr.library.ucar.edu/repository/assets/technotes/asset-000-000-000-848.pdf>
- Oleson, K. W., & Feddema, J. (2020). Parameterization and surface data improvements and new capabilities for the community land model urban (CLMU). *Journal of Advances in Modeling Earth Systems*, 12(2), 1–30. <https://doi.org/10.1029/2018MS001586>
- Oleson, K. W., Monaghan, A., Wilhelmi, O., Barlage, M., Brunsell, N., Feddema, J., Hu, L., & Steinhoff, D. F. (2015). Interactions between urbanization, heat stress, and climate change. *Climatic Change*, 129(3–4), 525–541. <https://doi.org/10.1007/s10584-013-0936-8>
- Opitz-Stapleton, S., Sabbag, L., Hawley, K., Tran, P., Hoang, L., & Nguyen, P. H. (2016). Heat index trends and climate change implications for occupational heat exposure in Da Nang, Vietnam. *Climate Services*, 2–3, 41–51. <https://doi.org/10.1016/j.ciser.2016.08.001>
- Orimoloye, I. R., Mazinyo, S. P., Nel, W., & Iortyom, E. T. (2017). Climate variability and heat stress index have increasing potential ill-health and environmental impacts in East London, South Africa. *International Journal of Applied Engineering Research*, 12 (17), 6910–6918. [http://danida.vnu.edu.vn/epis/files/Refs/Heat Waves/Heat\\_Stress/Climate Variability and Heat Stress Index have Increasing Potential Ill-health and Environmental Impacts in the East London, South Africa.pdf](http://danida.vnu.edu.vn/epis/files/Refs/Heat Waves/Heat_Stress/Climate Variability and Heat Stress Index have Increasing Potential Ill-health and Environmental Impacts in the East London, South Africa.pdf).
- Papalexiou, S. M., AghaKouchak, A., Trenberth, K. E., & Foufoula-Georgiou, E. (2018). Global, regional, and megacity trends in the highest temperature of the year: Diagnostics and evidence for accelerating trends. *Earth's Future*, 6(1), 71–79. <https://doi.org/10.1002/2017EF000709>
- Phelan, P. E., Kaloush, K., Miner, M., Golden, J., Phelan, B., Silva, H., & Taylor, R. A. (2015). Urban Heat Island: Mechanisms, implications, and possible remedies. *Annual Review of Environment and Resources*, 40(1), 285–307. <https://doi.org/10.1146/annurev-environ-102014-021155>
- Qiao, Y., Guo, Y., Stoner, A. M. K., & Santos, J. (2022). Impacts of future climate change on flexible road pavement economics: A life cycle costs analysis of 24 case studies across the United States. *Sustainable Cities and Society*, 80(February). <https://doi.org/10.1016/j.scs.2022.103773>
- Quah, A. K. L., & Roth, M. (2012). Diurnal and weekly variation of anthropogenic heat emissions in a tropical city, Singapore. *Atmospheric Environment*, 46, 92–103. <https://doi.org/10.1016/j.atmosenv.2011.10.015>
- Radeloff, V. C., Hammer, R. B., & Stewart, S. I. (2005). Rural and suburban sprawl in the U.S. Midwest from 1940 to 2000 and its relation to forest fragmentation. *Conservation Biology*, 19(3), 793–805. <https://doi.org/10.1111/j.1523-1739.2005.00387.x>
- Ramamurthy, P., & Sangobano, M. (2016). Inter-annual variability in urban heat island intensity over 10 major cities in the United States. *Sustainable Cities and Society*, 26, 65–75. <https://doi.org/10.1016/j.scs.2016.05.012>
- Raymond, C., Singh, D., & Horton, R. M. (2017). *Spatiotemporal patterns and synopses of extreme wet-bulb temperature in the contiguous*.
- Roth, M. (2007). Review of urban climate research in (sub)tropical regions. *International Journal of Climatology*, 27(27), 1859–1873.
- Rothfuss, L. P. (1990). The heat index equation (or, more than you ever wanted to know about heat index). *Fort Worth, Texas: National Oceanic and Atmospheric Administration, National Weather Service, Office of Meteorology*, 23–90. <https://c6bd9143-3623-4d4f-963f-62942ed32f11/Paper/p395>.
- Roy, S. S., & Yuan, F. (2009). Trends in extreme temperatures in relation to urbanization in the Twin Cities Metropolitan Area, Minnesota. *Journal of Applied Meteorology and Climatology*, 48(3), 669–679. <https://doi.org/10.1175/2008JAMC1983.1>
- Salimi, M., & Al-Ghamdi, S. G. (2020). Climate change impacts on critical urban infrastructure and urban resiliency strategies for the Middle East. *Sustainable Cities and Society*, 54, Article 101948. <https://doi.org/10.1016/j.scs.2019.101948>
- Santamouris, M. (2016). Urban Warming and Mitigation: Actual status, impacts and challenges. *Urban Climate Mitigation Techniques*. <https://doi.org/10.4324/9781315765839>
- Scott, G., Holland, A., & Sandifer, P. (2006). Afterword-managing coastal urbanization and development in the twenty-first century: The need for a new paradigm. *Changing Land Use Patterns in the Coastal Zone*, 285–299.
- Sen, K. P. (1968). Robustness of some nonparametric procedures in linear models. *The Annals of Mathematical Statistics*, 39(6), 1913–1922.
- Shaw, T. A., & Pauluis, O. (2012). Tropical and subtropical meridional latent heat transports by disturbances to the zonal mean and their role in the general circulation. *Journal of the Atmospheric Sciences*, 69(6), 1872–1889. <https://doi.org/10.1175/JAS-D-11-0236.1>
- Shen, C., Hou, H., Zheng, Y., Murayama, Y., Wang, R., & Hu, T. (2022). Prediction of the future urban heat island intensity and distribution based on landscape composition and configuration: A case study in Hangzhou. *Sustainable Cities and Society*, 83 (2318), Article 103992. <https://doi.org/10.1016/j.scs.2022.103992>
- Sherwood, S. C., & Huber, M. (2010). An adaptability limit to climate change due to heat stress. *Proceedings of the National Academy of Sciences of the United States of America*, 107(21), 9552–9555. <https://doi.org/10.1073/pnas.0913352107>
- Si, M., Li, Z. L., Nerry, F., Tang, B. H., Leng, P., Wu, H., Zhang, X., & Shang, G. (2022). Spatiotemporal pattern and long-term trend of global surface urban heat islands characterized by dynamic urban-extent method and MODIS data. *ISPRS Journal of Photogrammetry and Remote Sensing*, 183(October 2021), 321–335. <https://doi.org/10.1016/j.isprsjprs.2021.11.017>
- Silva, J. S., Silva, R. M., & Santos, C. A. G. (2018). Spatiotemporal impact of land use/land cover changes on urban heat islands: A case study of Paço do Lumiar, Brazil. *Building and Environment*, 136(March), 279–292. <https://doi.org/10.1016/j.buildenv.2018.03.041>
- Steadman, R. G. (1979). The assessment of sultriness. Part 1: A temperature-humidity index based on human physiology and clothing science. *Journal of Applied Meteorology*, 18, 861–873.
- Stewart, I. D., & Oke, T. R. (2012). Local climate zones for urban temperature studies. *Bulletin of the American Meteorological Society*, 93(12), 1879–1900. <https://doi.org/10.1175/BAMS-D-11-00019.1>
- Stone, B., Mallen, E., Rajput, M., Broadbent, A., Kravenhoff, E. S., Augenbroe, G., & Georgescu, M. (2021). Climate change and infrastructure risk: Indoor heat exposure during a concurrent heat wave and blackout event in Phoenix, Arizona. *Urban Climate*, 36(February), Article 100787. <https://doi.org/10.1016/j.ulclim.2021.100787>
- Suparta, W., & Yatim, A. N. M. (2017). An analysis of heat wave trends using heat index in East Malaysia. *Journal of Physics: Conference Series*, 852(1). <https://doi.org/10.1088/1742-6596/852/1/012005>
- Templeton, N. P., Vivoni, E. R., Wang, Z. H., & Schreiner-McGraw, A. P. (2018). Quantifying water and energy fluxes over different urban land covers in Phoenix, Arizona. *Journal of Geophysical Research: Atmospheres*, 123(4), 2111–2128. <https://doi.org/10.1002/2017JD027845>
- Tian, P., Li, J., Cao, L., Pu, R., Wang, Z., Zhang, H., Chen, H., & Gong, H. (2021). Assessing spatiotemporal characteristics of urban heat islands from the perspective of an urban expansion and green infrastructure. *Sustainable Cities and Society*, 74 (April), Article 103208. <https://doi.org/10.1016/j.scs.2021.103208>
- Vaidyanathan, A., Malilay, J., Schramm, P., & Saha, S. (2020). Heat-Related Deaths — United States, 2004–2018. 69(24). [https://www.cdc.gov/nchs/data/dvs/2e\\_volume1\\_2017.pdf](https://www.cdc.gov/nchs/data/dvs/2e_volume1_2017.pdf).
- Varquez, A. C. G., & Kanda, M. (2018). Global urban climatology: A meta-analysis of air temperature trends (1960–2009). *Npj Climate and Atmospheric Science*, 1(1), 1–8. <https://doi.org/10.1038/s41612-018-0042-8>
- Wang, R., Gao, W., Zhou, N., Kammen, M., & Peng, W. (2021a). Urban structure and its implication of heat stress by using remote sensing and simulation tool. *Sustainable Cities and Society*, 65(December 2020), Article 102632. <https://doi.org/10.1016/j.scs.2020.102632>
- Wang, S., Wu, C. Y. H., Richardson, M. B., Zaitchik, B. F., & Gohlke, J. M. (2021b). Characterization of heat index experienced by individuals residing in urban and rural settings. *Journal of Exposure Science and Environmental Epidemiology*, 31(4), 641–653. <https://doi.org/10.1038/s41370-021-00303-x>
- Watkins, R., Palmer, J., & Kolokotroni, M. (2007). Increased temperature and intensification of the urban heat island: Implications for human comfort and urban design. *Built Environment*, 33(1), 85–96. <https://doi.org/10.2148/benv.33.1.85>
- Webb, E. K., Pearman, G. I., & Leuning, R. (1980). Correction of flux measurements for density effects due to heat and water vapour transfer. *Quarterly Journal of the Royal Meteorological Society*, 106(447), 85–100. <http://onlinelibrary.wiley.com/doi/10.1002/qj.4910644707/abstract%0Apapers3://publication/uuid/D93C7190-B5B7-4657-9C9F-5868BDE5DFED>.
- Zander, K. K., Cadag, J. R., Escarcha, J., & Garnett, S. T. (2018). Perceived heat stress increases with population density in urban Philippines. *Environmental Research Letters*, 13(8). <https://doi.org/10.1088/1748-9326/aad2e5>
- Zhang, Q., Zhang, L., Huang, J., Zhang, L. Y., Wang, W. Y., & Sha, S. (2014). Spatial distribution of surface energy fluxes over the Loess Plateau in China and its relationship with climate and the environment. *Science China Earth Sciences*, 57(9), 2135–2147. <https://doi.org/10.1007/s11430-014-4881-9>
- Zhao, L., Lee, X., Smith, R. B., & Oleson, K. (2014). Strong contributions of local background climate to urban heat islands. *Nature*, 511(7508), 216–219. <https://doi.org/10.1038/nature13462>
- Zhao, L., Oppenheimer, M., Zhu, Q., Baldwin, J. W., Ebi, K. L., Bou-Zeid, E., Guan, K., & Liu, X. (2018). Interactions between urban heat islands and heat waves. *Environmental Research Letters*, 13(3). <https://doi.org/10.1088/1748-9326/aa973>